POLITECNICO DI TORINO
Repository ISTITUZIONALE

Comparison between collective coordinate models for domain wall motion in PMA nanostrips in the presence of the Dzyaloshinskii-Moriya interaction

(Article begins on next page)

18 April 2024

Accepted Manuscript

Comparison between collective coordinate models for domain wall motion in PMA nanostrips in the presence of the Dzyaloshinskii-Moriya interaction

J. Vandermeulen, S.A. Nasseri, B. Van de Wiele, G. Durin, B. Van Waeyenberge, L. Dupré

Comparison between collective coordinate models for domain wall motion in PMA nanostrips in the presence of the Dzyaloshinskii-Moriya interaction
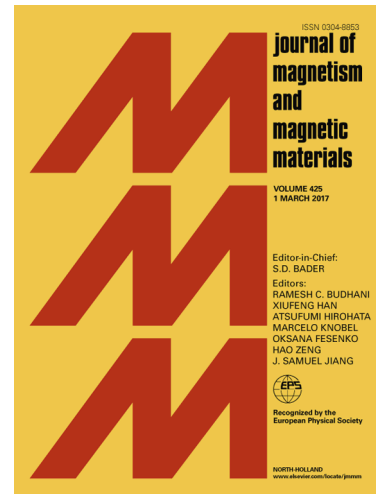
J. Vandermeulen[a,b,1,*], S. A. Nasseri[c,d,1,*], B. Van de Wiele[a], G. Durin[c,e], B. Van Waeyenberge[b], L. Dupré[a]

[a]*Department of Electrical Energy, Metals, Mechanical Constructions and Systems, Ghent University, Technologiepark 913, B-9052 Zwijnaarde, Belgium.*
[b]*Department of Solid State Sciences, Ghent University, Krijgslaan 281-S1, B-9000 Gent, Belgium.*
[c]*ISI Foundation, Via Alassio 11/c, 10126 Torino, Italy.*
[d]*Politecnico di Torino, Corso Duca degli Abruzzi 24, 10129 Torino, Italy.*
[e]*Istituto Nazionale di Ricerca metrologica, Strada delle Cacce 91, 10135 Torino, Italy.*

Abstract

Lagrangian-based collective coordinate models for magnetic domain wall (DW) motion rely on an ansatz for the DW profile and a Lagrangian approach to describe the DW motion in terms of a set of time-dependent collective coordinates: the DW position, the DW magnetization angle, the DW width and the DW tilting angle. Another approach was recently used to derive similar equations of motion by averaging the Landau-Lifshitz-Gilbert equation without any ansatz, and identifying the relevant collective coordinates afterwards. In this paper, we use an updated version of the semi-analytical equations to compare the Lagrangian-based collective coordinate models with micromagnetic simulations for field- and STT-driven (spin-transfer torque-driven) DW motion in Pt/CoFe/MgO and Pt/Co/AlO$_x$ nanostrips. Through this comparison, we assess the accuracy of the different models, and provide insight into the deviations of the models from simulations. It is found that the lack of terms related to DW asymmetry in the Lagrangian-based collective coordinate models significantly contributes to the discrepancy between the predictions of the most accurate Lagrangian-based model and the micromagnetic simulations in the field-driven case. This is in contrast to the STT-driven case where the DW remains symmetric.

1. Introduction

Manipulating magnetic domain walls (DWs) within nanostructures is essential for many applications in the development of spintronic logic [1–3], memory [4–6] and sensing devices [7]. Potential advantages of these and other devices which use magnetic moments to carry information include low power dissipation, non-volatile data retention, radiation hardness, faster manipulation of data, high areal densities and a reduced need for mechanical parts. These advantages have led to increased interest within the scientific community in qualitatively or quantitatively describing magnetic DW motion under applied fields and currents.

Both qualitative and quantitative descriptions rely on the Landau-Lifshitz-Gilbert (LLG) equation which expresses how the magnetization varies in space and time. In micromagnetic simulations, the ferromagnetic system is divided into many cells and the LLG equation is subsequently solved in each cell at every timestep, giving rise to a huge number of degrees of freedom. While this results in the most accurate description

of DW dynamics, more quantitative insight in DW dynamics is provided by theoretical models which describe the DW in terms of a limited number of variables. Here, we distinguish between Lagrangian-based [8–12] and semi-analytical [13–16] collective coordinate models (CCMs).

Lagrangian-based CCMs have the advantage that they are predictive and computationally very cost-effective; to evaluate the DW variables and the equations of motion, no micromagnetic simulations are needed. Moreover, they are very useful for early design analysis, conceptual studies or back-of-the-envelope calculations. The equations of motion typically rely on an ansatz which characterizes the spin texture of interest. Already in 1972, when micromagnetic simulation tools were not yet available, Slonczewski used a Lagrangian approach to propose the first collective coordinate model to analyze DW motion in perpendicularly magnetized materials (the $q - \phi$ model) [8]. This model relates the DW position q and supposedly uniform magnetization of the DW to the different magnetic interactions. The $q - \phi$ model is also called the 1D model, as the whole motion can be characterized by the in-plane magnetization angle ϕ.

Thiaville and Nakatani later extended this model to in-plane systems and introduced the DW width (Δ) as an additional time varying coordinate, leading to the $q - \phi - \Delta$ model [11]. Due to

---

*Corresponding authors
Email addresses:* `jasper.vandermeulen@ugent.be`
(J. Vandermeulen), `ali.nasseri@isi.it` (S. A. Nasseri)
[1]J. Vandermeulen and S. A. Nasseri contributed equally to this work.

the interest in current-driven DW motion at the time, the spin-transfer torque (STT) mechanism was also added to these models [9, 10].

Recent studies on heterostructures of ultrathin ferromagnets sandwiched between a heavy metal layer and an oxide have highlighted the importance of the Dzyaloshinskii-Moriya interaction (DMI) [17, 18], which stabilizes chiral DWs [19–22]. These chiral domains are of Néel or semi-Néel character depending on the strength of the DMI, while similar systems without this interaction will have Bloch DWs. The change in DW structure leads to extension of the Walker Breakdown towards higher excitation strengths [23], and also to tilting of the DW during motion [12]. While micromagnetic simulations of these heterostructures are in agreement with experiments [24], conventional Lagrangian-based CCMs ($q - \phi$ and $q - \phi - \Delta$) fail to reproduce the results [12, 25]. To overcome this issue, Boulle developed a tilted Lagrangian-based CCM (the $q - \phi - \chi$ model with χ the tilt angle of the DW in respect to the wire) to describe DW motion in PMA nanowires with DMI [12].

Since Lagrangian-based CCMs rely on an ansatz for the domain wall profile, they are inevitably limited by this constraint and do not describe the full details of DW dynamics. On the other hand, micromagnetic simulations which take the full complexity of DW dynamics into account, are hard to interpret. To bridge the gap between both, we recently introduced a semi-analytical approach to derive similar equations of motion for the DW which could be interpreted in the context of collective coordinates [13]. The earliest versions were able to succesfully describe DW dynamics in in-plane magnetized and PMA nanostrips, taking into account effects due to the finite temperature and disorder [13–15]. More recently, this approach was extended to account for DMI [16].

In this paper, we present a four collective coordinate model ($q - \phi - \chi - \Delta$) derived based on the Lagrangian approach. This model is compared to previous Lagrangian-based models. Using an improved semi-analytical approach, it is compared to micromagnetic simulations to assess its accuracy and to gain further understanding of the limitations of the models derived based on the Lagrangian approach.

2. The LLG and energy equation

Magnetization dynamics in ferromagnetic materials are governed by the Landau-Lifshitz-Gilbert (LLG) equation with additional terms added to account for other interactions such as the Spin Transfer Torque (STT). We follow the description developed by Berger [26] and refined by Zhang and Li [27] to account for this interaction. The full equation reads

$$\frac{\partial \mathbf{m}}{\partial t} = \frac{\gamma_0}{1 + \alpha^2} \mathbf{H}_{\text{eff}} \times \mathbf{m} + \frac{\alpha \gamma_0}{1 + \alpha^2} \mathbf{m} \times (\mathbf{H}_{\text{eff}} \times \mathbf{m})$$
$$+ \frac{\beta - \alpha}{1 + \alpha^2} \mathbf{m} \times (\mathbf{u} \cdot \nabla) \mathbf{m}$$
$$+ \frac{(1 + \alpha\beta)}{1 + \alpha^2} \mathbf{m} \times (\mathbf{m} \times ((\mathbf{u} \cdot \nabla) \mathbf{m})) \quad (1)$$

in which $\gamma_0 = \mu_0 \gamma$, with γ the gyromagnetic ratio and μ_0 the permeability of vacuum, $\mathbf{m} = \mathbf{M}/M_s$ is the normalized

magnetization vector with M_s the saturation magnetization, $\mathbf{H}_{\text{eff}} = -\frac{1}{\mu_0 M_s} \frac{\delta E}{\delta \mathbf{m}}$ with E the total energy is the effective magnetic field acting on the magnetization and α is the phenomenological Gilbert damping [28]. The second and third line in (1) include the adiabatic and non-adiabatic spin transfer torques (STTs) induced by the injection of spin polarized currents [10, 26, 27, 29–35]. We assume that the thickness of the magnetic layer is much larger than the heavy metal layer and hence, neglect the effect of spin orbit torques arising from the interface between the heavy metal layer and the ferromagnet. In the STT terms, β is the nonadiabaticity coefficient and $\mathbf{u} = -b_J \mathbf{J}$ with $b_J = \frac{P g \mu_B}{2(-e) M_s (1 + \beta^2)}$ is the velocity directed along the direction of electron motion, with $e = -1.602 \times 10^{-19} C$ the electron charge, g the Landé factor, μ_B the Bohr magneton, J denoting current density and P denoting the polarization rate of the current.

Finally, the effective field in equation (1) is related to the energy of the different interactions through $\mathbf{H}_{\text{eff}} = -\frac{1}{\mu_0 M_s} \frac{\delta E}{\delta \mathbf{m}}$. In the presence of an applied field, the total energy density of the system can be written as

$$E = A \sum_{i=1}^{3} \overbrace{|\nabla m_i|^2}^{\text{Exchange}} + \overbrace{K_0 + K_U m_{\text{ip}}^2}^{\text{Anisotropy}} - \overbrace{\frac{\mu_0 M_s}{2} \mathbf{H}_{\text{ms}} \cdot \mathbf{m}}^{\text{Magnetostatics}}$$
$$+ \overbrace{D(m_z \nabla \cdot \mathbf{m} - (\mathbf{m} \cdot \nabla) m_z)}^{\text{DMI}} - \overbrace{\mu_0 M_s \mathbf{H}_{\text{ext}} \cdot \mathbf{m}}^{\text{Zeeman}} \quad (2)$$

with $\mathbf{m}_{\text{ip}}$ the in-plane magnetization vector. Here, A is the exchange constant, K_0 is an anisotropy constant, K_U is the uniaxial anisotropy constant, $\mathbf{H}_{\text{ms}}$ is the demagnetizing field and $\mathbf{H}_{\text{ext}}$ is the externally applied field. The demagnetizing field can be calculated as $\mathbf{H}_{\text{ms}} = -\hat{N} \cdot M_s \mathbf{m}$ where $\hat{N}$ is the demagnetizing tensor. D is an uniform constant signifying the strength of the Dzyaloshinskii-Moriya interaction (DMI) with symmetries taken into account [23, 36, 37]. From equation (2), we derive that

$$\mathbf{H}_{\text{eff}} = -\frac{1}{\mu_0 M_s} \frac{\delta E}{\delta \mathbf{m}} \quad (3)$$
$$= \mathbf{H}_{\text{ext}} + \mathbf{H}_{\text{ani}} + \mathbf{H}_{\text{ms}} + \mathbf{H}_{\text{DMI}} + \mathbf{H}_{\text{exch}}$$

$$= \sum_{i=1}^{3} \overbrace{H_{\text{ext},i} \mathbf{e}_i}^{\text{external field}} + \overbrace{\frac{2K_U}{\mu_0 M_s^2} M_s m_z \mathbf{e}_z}^{\text{uniaxial anisotropy}} \overbrace{-\hat{N} \cdot M_s \mathbf{m}}^{\text{magnetostatic interaction}}$$

$$+ \overbrace{\frac{2D}{\mu_0 M_s} [\nabla m_z - (\nabla \cdot \mathbf{m}) \mathbf{e}_z]}^{\text{DMI}} + \overbrace{\frac{2A}{\mu_0 M_s} \sum_{i=1}^{3} \nabla^2 m_i \mathbf{e}_i}^{\text{exchange interaction}}.$$

3. The Lagrangian-based collective coordinate models

As illustrated in Fig. 1 (a), the normalized magnetization vector in spherical coordinates is expressed as

$$\mathbf{m} = (\cos \phi \sin \theta, \sin \phi \sin \theta, \cos \theta). \quad (4)$$

Using a Lagrangian approach, we switch from a description of the magnetization at every point in space and time (the LLG
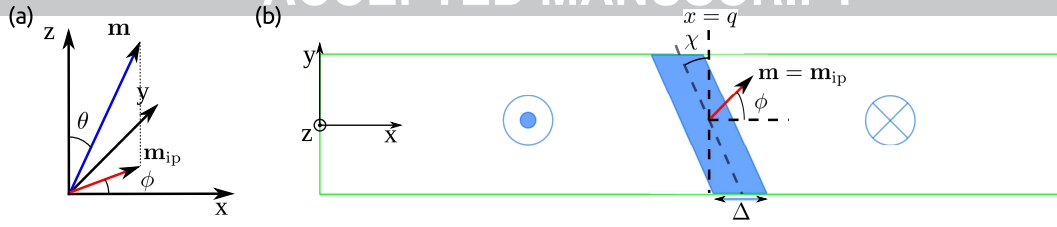
Figure 1: (a) The spherical coordinates ϕ and θ of the normalized magnetization vector $\mathbf{m}$ and its projection on the xy-plane, i.e. the in-plane magnetization vector $\mathbf{m}_{ip}$. (b) The collective coordinates used in the Lagrangian-based CCMs: the DW position q, the in-plane magnetization angle ϕ at the center of the DW ($\mathbf{m} = \mathbf{m}_{ip}$), the geometrical tilting angle χ and the DW width Δ.

equation given by (1)), to a description of more collective features of the DW. Based on micromagnetic simulations and experimental observations, the following time-dependent collective coordinates were identified for describing DW motion in such systems:

(i) The position of the center of the DW (q);

(ii) The in-plane magnetization angle at the center of the DW (ϕ);

(iii) The DW width (Δ); and

(iv) The tilt angle of the DW with respect to the width of the wire (χ).

The coordinates above are depicted in Fig. 1 (b). Hence, the three-dimensional DW dynamics is described as the dynamics of a point particle to which the collective coordinates are allocated. In other words, we remove the spatial dependence of DW dynamics. Different combinations of these coordinates have been previously used to derive Lagrangian-based CCMs for DW motion [8, 11, 12]. Here, all four coordinates are included in a single model.

In order to introduce a DW into the Lagrangian system of equations and switch from a description in the spatial coordinate system to one based on collective coordinates, the two coordinate systems need to be linked. Traditionally, the Bloch profile (derived based on consideration of exchange and anisotropy energies) has been used to relate the local coordinates with the collective coordinates [8, 11]. Studies on PMA systems with DMI have shown that this profile can be used in these systems as well [22]. Here, we use a tilted version of this ansatz [12]

$$
\begin{cases}
\theta(x, y, t) & = 2 \arctan\left[\exp\left(\frac{(x-q(t))\cos\chi(t)+y\sin\chi(t)}{\Delta(t)}\right)\right] \\
\phi(x, y, t) & = \phi(t).
\end{cases}
\tag{5}
$$

along with the assumption that the direction of the in-plane component of magnetization $\mathbf{m}_{ip}$ is uniform inside the DW. Using this ansatz, θ ranges from 0 to π (which is equivalent to m_z going from 1 to -1). Introducing this ansatz constrains the magnetization dynamics in order to maintain the DW as a rigid object. This is not necessarily the case, especially near the edges of the nanowire. However, this assumption is justified since we show in AppendixD that the edge effects have a rather small effect on the equations of motion.

For simplicity, this paper will only use the form of the ansatz presented above. When the left domain is pointing along the negative z-direction, the ansatz needs to be adjusted to $\theta(x, y, t) = 2 \arctan\left[\exp\left(-\frac{(x-q(t))\cos\chi(t)+y\sin\chi(t)}{\Delta(t)}\right)\right]$, which will affect some of the terms in the equations. Alternatively, the coordinate system may be rotated to find equivalent equations for the motion of the DW. Moreover, we also assume that the magnetization inside the DW points along the positive x-direction without excitation, which is valid for a large enough DMI strength ($D < 0$) (cases studied in this paper). For cases where $D > 0$ and larger than a threshold value, the coordinate ϕ should be replaced by $\pi + \phi$ to take the initial configuration of the DW into account. In this case, the ansatz for θ does not change.

The demagnetizing factors used in the model may be calculated based on the geometry of the system using ellipsoidal approximations of the DW volume [38]. As a consequence of this ellipsoidal approximation, the demagnetizing factors act on the DW through the ($\phi - \chi$)-angle instead of the magnetization angle (ϕ).

To remove the spatial dependence of the energy terms, the Lagrangian and dissipation function of the system are integrated in the x and y direction using the ansatz. In AppendixA, the equations of motion of the four collective coordinate model are listed along with more details about the derivation of these equations and the differences with the equations of motion of other Lagrangian-based CCMs.

4. The semi-analytical approach

Alternatively, a semi-analytical model can be developed [16], based on averaging the LLG-equation. To this end, the *locally* varying effective field (3) is first properly averaged *over the DW volume* and substituted in the LLG equation. Then, the LLG equation is again averaged over the domain wall volume to obtain equations of motion with DW variables which are quantified by extracting them from simulations. Compared to our initial model [16], the semi-analytical approach is now improved to properly treat the effects of the DW asymmetry on the DW dynamics. In AppendixB, the semi-analytical approach and the derivation of the equations of motion are discussed in detail. Moreover, the DW variables extracted from the equations of motion are also discussed. Apart from the DW position Q, the averaged in-plane DW magnetization angle Φ_{av} and its in-plane

3

weighted variant $\Phi_{\text{av,w}}$ are identified as well as the DW width Δ_{av} and the geometrical tilting angle X_{av}. Furthermore, we identify DW variables κ_{av} and its in-plane weighted variant $\kappa_{\text{av,w}}$ describing the DW shape (AppendixC). We also identify three exchange related DW variables $g_{x,\text{av}}$, $g_{y,\text{av}}$ and $g_{z,\text{av}}$. The effective demagnetizing factors $N_{\text{eff},x}$, $N_{\text{eff},y}$ and $N_{\text{eff},z}$ are determined from micromagnetic simulations as detailed in AppendixB.

To ensure that the semi-analytical equations of motion are in accordance with the micromagnetic simulations, we made an assessment of the semi-analytical model with micromagnetic simulations in AppendixD. Micromagnetic simulations were executed for both field-driven DW dynamics in Pt/CoFe/MgO and STT-driven DW dynamics in Pt/Co/AlO$_x$ as detailed in Subsection 5.2.

5. Comparison between the Lagrangian-based collective coordinate models and the semi-analytical model

5.1. The equations of motion

To enable a comparison between the Lagrangian-based CCMs and micromagnetic simulations, we use the semi-analytical approach and link the equations of motion in the semi-analytical approach with those in the four coordinate model. The velocity equation from both the semi-analytical approach and the four coordinate Lagrangian-based model can be written as

$$
\begin{aligned}
\frac{1+\alpha^2}{\gamma_0}\frac{1}{P_\Delta}v =& \alpha H_{\text{ext},z} + \frac{1+\alpha\beta}{\gamma_0}\frac{1}{P_\Delta}u_x \\
&+ \frac{1}{P_{\kappa,\text{field}}}\left[H_{\text{ext},x}\sin P_\phi - H_{\text{ext},y}\cos P_\phi\right] \\
&+ M_s P_{\text{ms}} \\
&- \frac{2D}{\mu_0 M_s}\frac{1}{P_\Delta}P_{\kappa,\text{DMI}}\left[\sin P_\phi - \tan P_\chi \cos P_\phi\right] \\
&+ \frac{2A}{\mu_0 M_s}P_{\text{exch}} \\
&+ \frac{1+\alpha^2}{\gamma_0}\frac{1}{P_\Delta}P_{\text{asym},v,1}
\end{aligned}
\tag{6}
$$

with the specific definition of the different parameters listed in Table 1.

Similarly, the change in magnetization angle can be written as

$$
\begin{aligned}
\frac{1+\alpha^2}{\gamma_0}\dot{\Phi} =& H_{\text{ext},z} + \frac{\beta-\alpha}{\gamma_0}\frac{1}{P_\Delta}u_x \\
&- \frac{\alpha}{P_{\kappa,\text{field}}}\left[H_{\text{ext},x}\sin P_\phi - H_{\text{ext},y}\cos P_\phi\right] \\
&- \alpha M_s P_{\text{ms}} \\
&+ \alpha\frac{2D}{\mu_0 M_s}\frac{1}{P_\Delta}P_{\kappa,\text{DMI}}\left[\sin P_\phi - \tan P_\chi \cos P_\phi\right] \\
&- \alpha\frac{2A}{\mu_0 M_s}P_{\text{exch}} \\
&+ P_{\text{asym},H_{\text{ext},z}},
\end{aligned}
\tag{7}
$$

while both equations can be combined to

$$
v + \frac{1}{\alpha}P_\Delta\dot{\Phi} = \frac{\gamma_0}{\alpha}P_\Delta H_{\text{ext},z} + \frac{\beta}{\alpha}u_x + P_{\text{asym},v,2}.
\tag{8}
$$

In the semi-analytical model,

$$
\dot{\Phi} = \frac{\langle m_{\text{ip}}^2 \frac{\partial \phi}{\partial t}\rangle}{\langle m_{\text{ip}}^2\rangle}
\tag{9}
$$

with $\mathbf{m}_{\text{ip}}$ the in-plane magnetization vector and ϕ the local in-plane magnetization angle. On the other hand, $\dot{\Phi} = \dot{\phi}$ in the Lagrangian-based CCMs with ϕ the uniform in-plane magnetization angle. Table 1 shows that, while the terms related to the Zeeman term are identical in both approaches, there are differences in the two descriptions in terms of magnetostatic terms. Furthermore, we can also assume that $\Phi_{\text{av,w}} \approx \Phi_{\text{av}}$ as outlined in AppendixD. Hence, demagnetizing terms in the semi-analytical model can be simplified to

$$
\begin{aligned}
&\frac{\kappa_{\text{av,w}}}{\kappa_{\text{av}}}\left[N_{\text{eff},y}\sin\Phi_{\text{av,w}}\cos\Phi_{\text{av}} - N_{\text{eff},x}\cos\Phi_{\text{av,w}}\sin\Phi_{\text{av}}\right] \\
&\approx \frac{\kappa_{\text{av,w}}}{\kappa_{\text{av}}}\left(N_{\text{eff},y} - N_{\text{eff},x}\right)\frac{\sin 2\Phi_{\text{av}}}{2}.
\end{aligned}
\tag{10}
$$

Now, the difference between the magnetostatic terms in both models is clear: while the semi-analytical model takes the effect of changes in the DW plane into account by both a scaling factor $\frac{\kappa_{\text{av,w}}}{\kappa_{\text{av}}}$ related to the DW shape and effective demagnetizing factors extracted from micromagnetic simulations, the Lagrangian-based model takes this change into account as a change in the effective angle the spin makes with the line $m_z = 0$. Another observation is that the value of κ_{av} from the semi-analytical approach is predicted to be $\frac{\pi}{4} \approx 0.7854$ and $\frac{2}{\pi} \approx 0.6366$ when comparing the prefactors κ_{DMI} from the DMI terms and κ_{field} from the in-plane field terms, respectively. In AppendixC, we show that κ_{av} is a value between 0 and 1 and that κ_{av} depends on the domain wall shape, i.e. the change of m_z over the DW profile. We calculate that $\kappa_{\text{av}} = \frac{2}{\pi} = \kappa_{\text{field}}$ after substituting the m_z-value of (4) in the expression for κ_{av} and using the ansatz (5) of the Lagrangian-based CCMs. It is also notable that the semi-analytical model has additional terms related to exchange and asymmetry which do not exist in the Lagrangian-based CCMs. DW asymmetry is rigorously defined in AppendixB.

5.2. Numerical comparison

5.2.1. Introduction

Now, we compare the collective coordinate models with micromagnetic simulations, using the semi-analytical model to better understand the underlying reason for the shortcomings of these models. We distinguish between four different collective coordinate models: the $q - \phi$, the $q - \phi - \Delta$, the $q - \phi - \chi$ and the $q - \phi - \chi - \Delta$ model. Using the micromagnetic software package MuMax^3[39], we study field-driven DW dynamics in Pt/CoFe/MgO and STT-driven DW dynamics in Pt/Co/AlO$_x$. Typical material parameters are listed in Table 2. The cross sectional dimensions of the simulated magnetic CoFe and Co

4

	$q - \phi - \chi - \Delta$	semi-analytical
P_Δ	$\frac{\Delta}{\cos\chi}$	$\frac{\Delta_{\text{av}}}{2}$
P_ϕ	ϕ	Φ_{av}
$P_{\kappa,\text{DMI}}$	$\kappa_{\text{DMI}} = \pi/4$	κ_{av}
$P_{\kappa,\text{field}}$	$\kappa_{\text{field}} = 2/\pi$	
P_χ	χ	X_{av}
P_{ms}	$\left(N_y - N_x\right)\frac{\sin 2(\phi-\chi)}{2}$	$\frac{\kappa_{\text{av,w}}}{\kappa_{\text{av}}}\left[N_{\text{eff},y} \sin \Phi_{\text{av,w}} \cos \Phi_{\text{av}} - N_{\text{eff},x} \cos \Phi_{\text{av,w}} \sin \Phi_{\text{av}}\right]$
P_{exch}	0	$g_{x,\text{av}} \sin \Phi_{\text{av}} - g_{y,\text{av}} \cos \Phi_{\text{av}}$
$P_{\text{asym},v,1}$		$O_{v,1}(\text{asymmetric})$
$P_{\text{asym},v,2}$	0	$O_{v,2}(\text{asymmetric})$
$P_{\text{asym},H_{\text{ext},z}}$		$O_{H_{\text{ext},z}}(\text{asymmetric})$

Table 1: Definition of the parameters in equations (6), (7) and (8) expressing the DW velocity and the change in magnetization angle in the four collective coordinate model and the semi-analytical model.

	Pt/CoFe/MgO	Pt/Co/AlO$_x$
M_s (A/m)	700×10^3	1090×10^3
A (J/m)	1×10^{-11}	1.6×10^{-11}
K_U (J/m^3)	0.48×10^6	1.25×10^6
α	0.3	0.5
D (mJ/m^2)	-1.2	-2.2
β	-	1.7

Table 2: Typical material parameters for Pt/CoFe/MgO nanostrips [25, 40] and for Pt/Co/AlO$_x$ nanostrips [41, 42].

nanostrips were 160×0.6 nm^2 while the simulation window was restricted to an area of length 640 nm following the DW in its propagation through an infinite nanostrip. The discretization cells had dimensions $1.25 \times 1.25 \times 0.6$ nm^3. This is not too large since in Pt/CoFe/MgO $\sqrt{A/K} \approx 4.56$ nm and in Pt/Co/AlO$_x$ $\sqrt{A/K} \approx 3.58$ nm. Note that, when calculating the averages in the semi-analytical approach, interpolation was used to compensate for discretization effects as discussed in AppendixE.

In general, one can discriminate between two propagation regimes of a DW, separated by the Walker Breakdown (WB) [43]. Below the WB, the DW adapts itself to the perpendicularly applied field or the applied current along the length of the nanostrip, resulting in a steady state translational motion along the nanostrip. In the equations of motion, this corresponds to

$$\dot{\Phi} = 0, \tag{11}$$

implying a fixed magnetization of the DW. In fact, all DW variables except for the DW position, are constant. This way, we can also rewrite equation (7) as a function of the excitation. The resulting equation then expresses how the different interaction contributions add up to balance the excitation. As long as these interactions can balance the excitation, we are below the WB. In this paper, we limit the discussion to DW dynamics below the WB.

5.2.2. Field-driven DW dynamics

In Figure 2, the collective coordinates of the Lagrangian-based CCMs (the $q - \phi$, $q - \phi - \Delta$, $q - \phi - \chi$ and the $q - \phi - \chi - \Delta$

models) for field-driven DW motion in a Pt/CoFe/MgO nanostrip are compared to micromagnetic simulations processed using the semi-analytical approach. Due to the similarity between the $q - \phi - \chi$ and the $q - \phi - \chi - \Delta$ model predictions on one hand and the $q - \phi$ and the $q - \phi - \Delta$ predictions on the other hand, we simplify the discussion by distinguishing between two types of models: those that include χ and those that do not. The χ-models clearly overestimate the DW velocity while the other models underestimate the DW velocity. Furthermore, we observe that the χ-models slightly overestimate ϕ and χ, while ϕ is strongly underestimated by the models that do not include χ. Surprisingly, all models predict $\phi - \chi$ with great accuracy. On the other hand, the χ-models overestimate the scaled DW width, while the other Lagrangian-based CCMs strongly underestimate the DW width. This is the main reason for the overestimation of the DW velocity by the χ-models and its underestimation by the other Lagrangian-based CCMs. We also calculated the normalized root mean-square error NRMSE and the coefficient of determination R^2 for this comparison in Table 3.

To enable a more in-depth comparison, Figure 3 compares the differences in how the interactions are estimated between the semi-analytical model and their Lagrangian-based counterparts as listed in Table 1. We observe that the influence of DMI is overestimated by the Lagrangian-based CCMs, which is clear in combination with equations (6) and (7). The differences between the terms that express the magnetostatic contribution to the DW dynamics are clear from Subsection 5.1, thereby taking into account that $\frac{\kappa_{\text{av,w}}}{\kappa_{\text{av}}}$ varies between 1.08 and 1.1. We also observe that the absolute value of the sum of the asymmetric contributions to the DW velocity and the out-of-plane field $\mu_0 H_{\text{ext},z}$ typically increase as a function of the out-of-plane field. These asymmetric contributions slow the DW down, thereby increasing the Walker Breakdown field. Following equation (8), this is an additional reason for the overestimation of the DW velocity by the Lagrangian-based χ-models, which do not consider asymmetry. On the other hand, the exchange contribution tends to decrease the Walker Breakdown field at large excitation strengths.
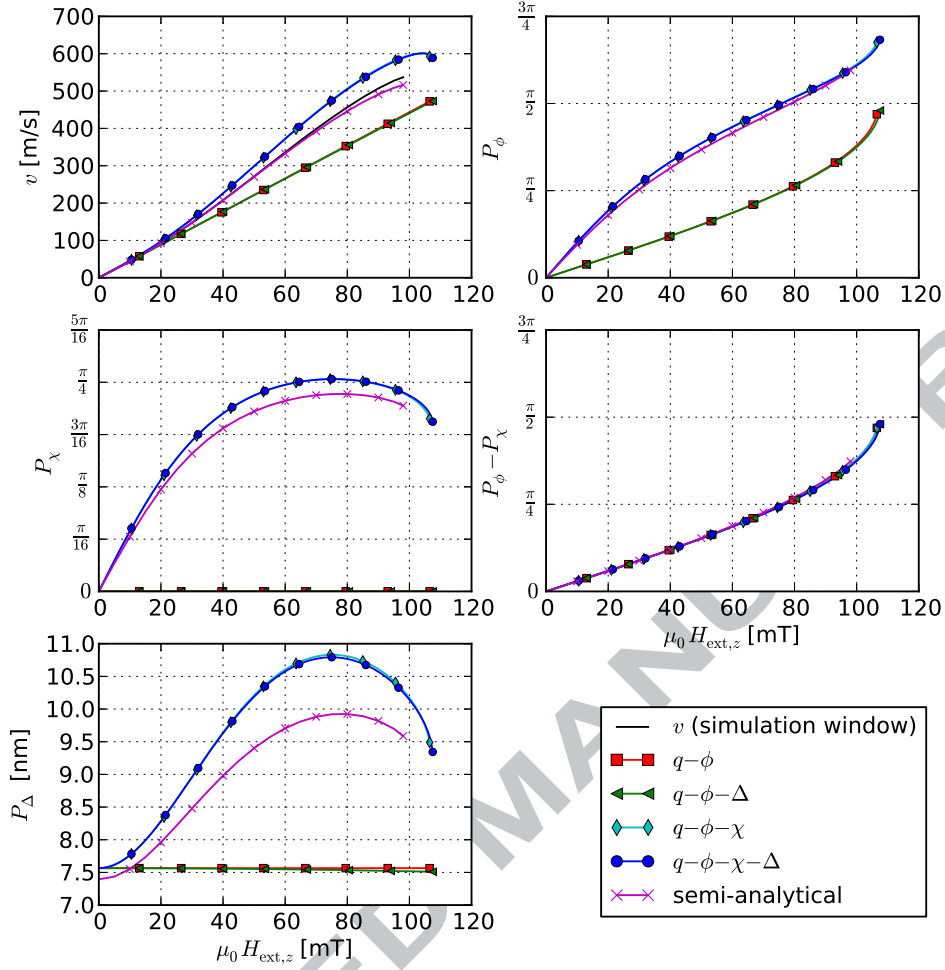
Figure 2: Comparison of the velocity and the collective coordinates (see Table 1) of the Lagrangian-based CCMs (the $q-\phi$, $q-\phi-\Delta$, $q-\phi-\chi$ and the $q-\phi-\chi-\Delta$ models) with micromagnetic simulations using the semi-analytical approach for <u>field-driven</u> DW motion in a Pt/CoFe/MgO nanostrip. The DW velocity as determined by the built-in simulation window velocity of MuMax[3] is plotted as a black line in the top-left part.

Model	Velocity NRMSE [R^2]	P_ϕ NRMSE [R^2]	P_χ NRMSE [R^2]	$P_\phi - P_\chi$ NRMSE [R^2]	P_Δ NRMSE [R^2]
$q-\phi$	24.31% [85.56%]	56.61% [-]	-	2.14% [99.9%]	18.82% [-]
$q-\phi-\Delta$	24.69% [85.11%]	56.91% [-]	-	3.01% [99.8%]	19.04% [-]
$q-\phi-\chi$	12.44% [96.22%]	3.96% [99.39%]	8.71% [95.3%]	2.14% [99.9%]	7.62% [42.69%]
$q-\phi-\chi-\Delta$	12.02% [96.47%]	3.79% [99.44%]	8.74% [95.26%]	3.01% [99.8%]	7.36% [46.6%]

Table 3: The normalized root mean square error (NRMSE) and coefficient of determination R^2 of the collective coordinate models (the $q-\phi$, $q-\phi-\Delta$, $q-\phi-\chi$ and $q-\phi-\chi-\Delta$ models) as compared to micromagnetic simulations using the semi-analytical approach for <u>field-driven</u> DW motion in a Pt/CoFe/MgO nanostrip. More specifically, the predicted DW velocity is compared to the built-in simulation window velocity of MuMax[3], while the parameters P_ϕ, P_χ, $P_\phi - P_\chi$ and P_Δ from the Lagrangian-based CCMs and the semi-analytical model are compared. These parameters are defined in Table 1.
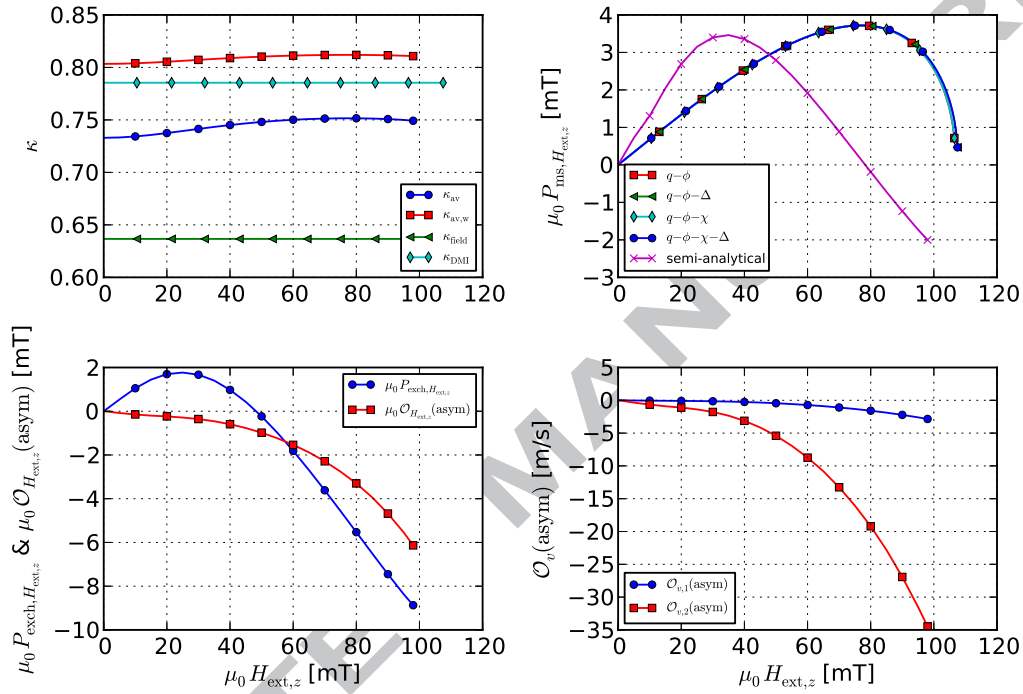
6

Figure 3: Comparison of differences between Lagrangian-based CCMs and micromagnetic simulations in addition to the differences depicted in Fig. 2 for field-driven DW motion in a Pt/CoFe/MgO nanostrip, thereby taking Table 1 into account. From top-left to bottom-right: the DW shape factors κ (κ_{av} and $\kappa_{\text{av,w}}$ from the semi-analytical model with κ_{field} and κ_{DMI} from the Lagrangian-based CCMs), the magnetostatic contribution $\mu_0 P_{\text{ms},H_{\text{ext},z}}$ ($P_{\text{ms},H_{\text{ext},z}} = \alpha M_{\text{s}} P_{\text{ms}}$) to the out-of-plane field $\mu_0 H_{\text{ext},z}$, the exchange contribution $\mu_0 P_{\text{exch},H_{\text{ext},z}}$ ($P_{\text{exch},H_{\text{ext},z}} = \alpha \frac{2A}{\mu_0 M_{\text{s}}} P_{\text{exch}}$) and asymmetric contribution $\mu_0 O_{H_{\text{ext},z}}$(asymmetric) to $\mu_0 H_{\text{ext},z}$ and the asymmetric contributions $O_{v,1}$(asymmetric) and $O_{v,2}$(asymmetric) to the DW velocity.

7

5.2.3. STT-driven DW dynamics

In Figure 4, the collective coordinates of the Lagrangian-based CCMs (the $q-\phi$, $q-\phi-\Delta$, $q-\phi-\chi$ and the $q-\phi-\chi-\Delta$ models) for STT-driven DW motion in a Pt/Co/AlO$_x$ nanostrip are compared to micromagnetic simulations using the semi-analytical approach. We observe that the DW velocity is much better predicted by all models compared to the field-driven case. While there are still significant discrepancies between the models that do not include χ and micromagnetic simulations, the χ-models are generally in much better correspondence with the micromagnetic simulations than in the field-driven case. The DW width is still slightly overestimated by the χ-models, but the discrepancy is significantly smaller. Moreover, the prediction of the DW tilting angle is also significantly improved. ϕ and $\phi-\chi$ are now clearly underestimated by the χ-models. In contrast to the field-driven case, the prediction of $\phi-\chi$ by the other Lagrangian-based CCMs is significantly worse. We also calculated the normalized root mean-square error NRMSE and coefficient of determination R^2 for this comparison in Table 4.

Fig. 5 shows why the collective coordinates are generally better predicted by the χ-models compared to the field-driven case: the asymmetric and exchange contributions to the DW dynamics are almost negligible and these contributions are not properly taken into account by the equations of motion of the Lagrangian-based CCMs.

6. Conclusion

In this paper, we compared the Lagrangian-based CCMs with micromagnetic simulations using a semi-analytical approach for field-driven and STT-driven DW motion in Pt/CoFe/MgO and Pt/Co/AlO$_x$ nanostrips. Lagrangian-based CCMs have the advantage of computational efficiency and ease of use, while their simplicity means losing part of the full picture. The semi-analytical model helps understand these shortcomings, and can be used to identify cases where the Lagrangian-based models might not be appropriate for use.

We introduced a four collective coordinate Lagrangian-based model, while models in literature describe DW motion with two or three collective coordinates [8, 11, 12]. The equations of motion of the four collective coordinate model and an improved semi-analytical approach were linked to enable the comparison with micromagnetic simulations. From this comparison, it is clear that the models that include the tilting angle χ are generally in much better correspondence with micromagnetic simulations than the models that do not include χ. Moreover, the Lagrangian-based CCMs predict the DW dynamics much better in the STT-driven case than in the field-driven case. The main reason for this is that, while asymmetric and exchange contributions to the DW dynamics are not properly taken into account by the equations of motion of the analytical CCMs, these contributions are almost negligible in the STT-driven case, but significant in the field-driven case.

While in this paper, the comparison between the Lagrangian-based CCMs and micromagnetic simulations using the semi-analytical approach was limited to two specific cases, this work demonstrates a tool that is in general applicable. This way, a comparison between analytical CCMs and micromagnetic simulations can also be done for nanostrips with other dimensions and/or from other materials. Moreover, this work could inspire researchers to further improve existing Lagrangian-based CCMs, e.g. by including asymmetry in the ansatz of the DW profile.

AppendixA. The four collective coordinate model

In Section 3, the collective coordinates and the ansatz for the DW profile are introduced. Here, we list the equations of motion of the four collective coordinate model along with details about the derivation of these equations and the differences with the equations of motion of other Lagrangian-based CCMs.

Using a Lagrangian approach, we change from a description of the magnetization at every point in space and time (the LLG equation given by (1)), to a description of more collective features of the DW. It can be shown that the following Lagrangian density ($\mathcal{L}$) and dissipation density ($\mathcal{F}$) functions can be used in the Euler-Lagrange equation to derive the LLG equation [12]

$$\mathcal{L} = E + \overbrace{\frac{M_s}{\gamma}\dot{\phi}\cos\theta}^{\text{Precessional Term}} - \overbrace{\frac{uM_s}{\gamma}\phi\frac{\partial(\cos\theta)}{\partial x}}^{\text{STT}} \tag{A.1}$$

and

$$\mathcal{F} = \frac{\alpha M_s}{2\gamma}\left[\frac{\partial \mathbf{m}}{\partial t} + \frac{\beta}{\alpha}(\mathbf{u}\cdot\nabla)\mathbf{m}\right]^2 \tag{A.2}$$

with E given by equation (2).

To evaluate DW dynamics using the collective coordinates, the energy terms and dissipation function are rewritten in terms of the collective coordinates, and integrated over the DW profile along the length and width of the nanowire. The properties of the ansatz help simplify the integration process. The Lagrangian and dissipation functions derived after integration are plugged into the Euler-Lagrange equations to derive the equations of motion for the rigid DW.
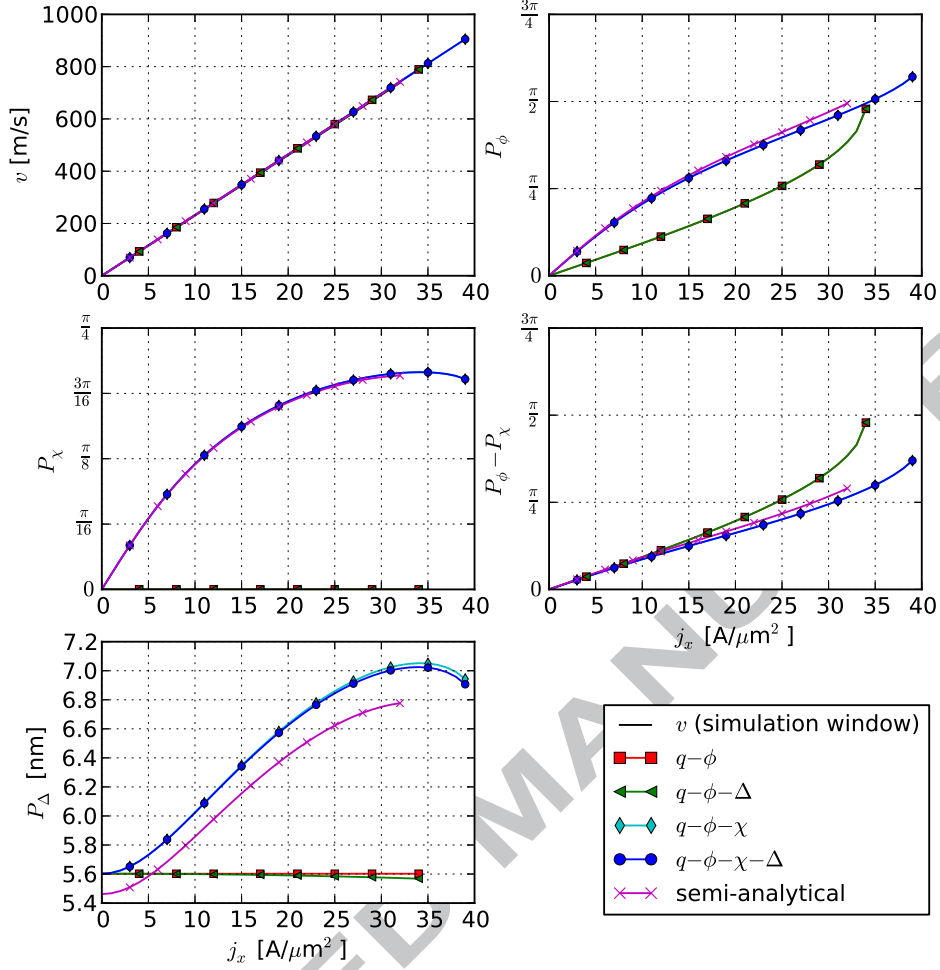
Figure 4: Comparison of the velocity and the collective coordinates (see Table 1) of the Lagrangian-based CCMs (the $q - \phi$, $q - \phi - \Delta$, $q - \phi - \chi$ and the $q - \phi - \chi - \Delta$ models) with micromagnetic simulations using the semi-analytical approach for <u>STT-driven</u> DW motion in a Pt/Co/AlO$_x$ nanostrip. The DW velocity as determined by the built-in simulation window velocity of MuMax^3 is plotted as a black line in the top-left part.

Model	Velocity NRMSE [R^2]	P_ϕ NRMSE [R^2]	P_χ NRMSE [R^2]	$P_\phi - P_\chi$ NRMSE [R^2]	P_Δ NRMSE [R^2]
$q - \phi$	0.89% [99.98%]	44.75% [21.14%]	-	24.17% [82.91%]	11.67% [-]
$q - \phi - \Delta$	0.89% [99.98%]	44.74% [21.14%]	-	24.18% [82.89%]	11.89% [-]
$q - \phi - \chi$	0.89% [99.98%]	4.08% [99.34%]	0.81% [99.96%]	8.9% [97.68%]	3.27% [80.17%]
$q - \phi - \chi - \Delta$	0.89% [99.98%]	4.08% [99.34%]	0.81% [99.97%]	8.9% [97.68%]	3.11% [81.99%]

Table 4: The normalized root mean square error (NRMSE) and coefficient of determination R^2 of the collective coordinate models ($q - \phi$, $q - \phi - \Delta$, $q - \phi - \chi$ and $q - \phi - \chi - \Delta$) as compared to micromagnetic simulations using the semi-analytical approach for <u>STT-driven</u> DW motion in a Pt/Co/AlO$_x$ nanostrip. More specifically, the predicted DW velocity is compared to the built-in simulation window velocity of MuMax^3, while the parameters P_ϕ, P_χ, $P_\phi - P_\chi$ and P_Δ from the Lagrangian-based CCMs and the semi-analytical model are compared. These parameters are defined in Table 1.
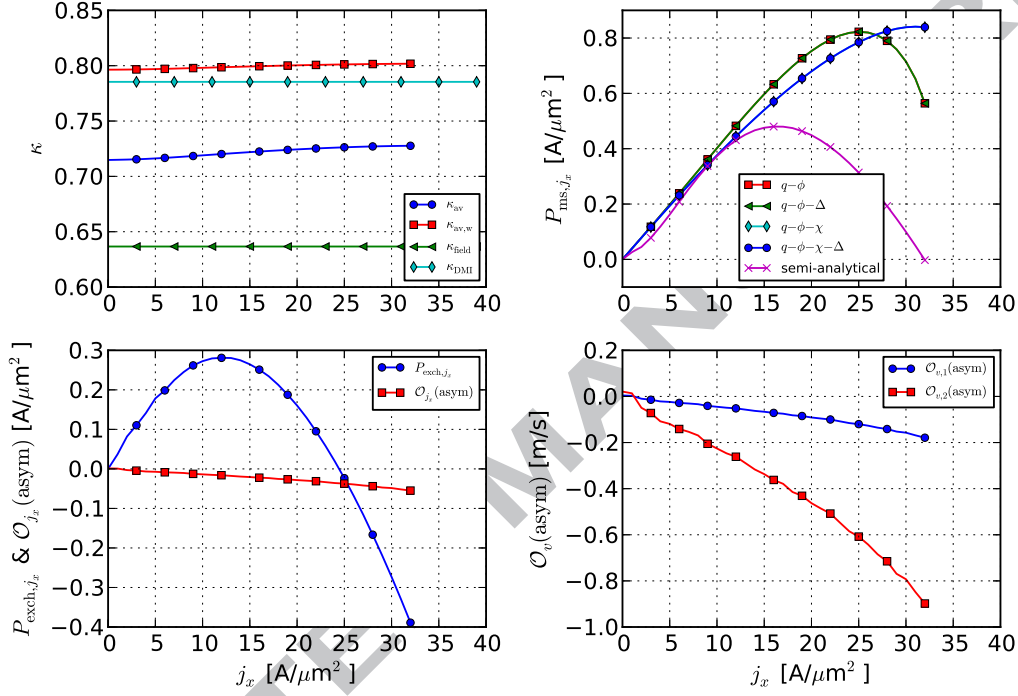
9

Figure 5: Comparison of differences between Lagrangian-based CCMs and micromagnetic simulations in addition to the differences depicted in Fig. 4 for <u>STT-driven</u> DW motion in a Pt/Co/AlO$_x$ nanostrip, thereby taking Table 1 into account. From top-left to bottom-right: the DW shape factors κ (κ_{av} and $\kappa_{av,w}$ from the semi-analytical model with κ_{field} and κ_{DMI} from the Lagrangian-based CCMs), the magnetostatic contribution P_{ms,j_x} ($P_{ms,j_x} = \frac{\alpha\gamma_0}{\beta-\alpha}\frac{P_\Delta}{-b_J}M_s P_{ms}$) to the current density j_x, the exchange contribution P_{exch,j_x} ($P_{exch,j_x} = \frac{\alpha\gamma_0}{\beta-\alpha}\frac{P_\Delta}{-b_J}\frac{2A}{\mu_0 M_s}P_{exch}$) and asymmetric contribution O_{j_x}(asymmetric) to j_x and the asymmetric contributions $O_{v,1}$(asymmetric) and $O_{v,2}$(asymmetric) to the DW velocity.

10

The first two equations derived using this approach by taking derivatives with respect to the conjugate coordinates q and ϕ are

$$
\begin{aligned}
\frac{\left(1+\alpha^2\right)}{\gamma_0}\frac{\cos\chi}{\Delta}\dot{q} =\,&\alpha H_{\text{ext},z} + \frac{\cos\chi}{\Delta}\frac{(1+\alpha\beta)}{\gamma_0}u \\
&+ \frac{\pi}{2}\left[H_{\text{ext},x}\sin\phi - H_{\text{ext},y}\cos\phi\right] \\
&+ \frac{1}{2}M_s\left(N_y - N_x\right)\sin\left(2(\phi - \chi)\right) \\
&- \frac{\pi}{2}\frac{D}{\mu_0 M_s \Delta}\sin\left(\phi - \chi\right)
\end{aligned} \tag{A.3}
$$

and

$$
\begin{aligned}
\frac{\left(1+\alpha^2\right)}{\gamma_0}\dot{\phi} =\,&H_{\text{ext},z} + \frac{\cos\chi}{\Delta}\frac{\beta-\alpha}{\gamma_0}u \\
&- \alpha\frac{\pi}{2}\left[H_{\text{ext},x}\sin\phi - H_{\text{ext},y}\cos\phi\right] \\
&- \frac{\alpha}{2}M_s\left(N_y - N_x\right)\sin\left(2(\phi-\chi)\right) \\
&+ \alpha\frac{\pi}{2}\frac{D}{\mu_0 M_s \Delta}\sin\left(\phi - \chi\right).
\end{aligned} \tag{A.4}
$$

The equations for the evolution of the two other conjugate collective coordinates, χ and Δ, are

$$
\begin{aligned}
\frac{\pi^2}{12}\alpha\frac{\dot{\Delta}}{\Delta} =\,&\frac{\gamma}{M_s}\left[\frac{A}{\Delta^2} - K_U + \frac{\mu_0 M_s^2}{2}N_z\right] \\
&- \frac{\gamma}{M_s}\frac{\mu_0 M_s^2}{2}\left[N_x\cos^2\left(\phi-\chi\right) + N_y\sin^2\left(\phi-\chi\right)\right] \\
&+ \frac{\pi}{2}\gamma_0\left(H_{\text{ext},x}\cos\phi + H_{\text{ext},y}\sin\phi\right) \\
&+ \frac{\gamma}{M_s}\left(\frac{\pi\Delta}{L_y}\right)^2\sin\chi\left[2\frac{A}{\Delta^2}\sin\chi + \frac{\pi}{2}\frac{D}{\Delta}\sin\phi\right] \\
&- \frac{\gamma}{M_s}\left(\frac{\pi\Delta}{L_y}\right)^2\frac{\sin 2\chi}{2}\frac{\mu_0 M_s^2}{2}\left(N_y - N_x\right)\sin\left(2(\phi-\chi)\right)
\end{aligned} \tag{A.5}
$$

and

$$
\begin{aligned}
-\frac{\pi^2}{12}\frac{\alpha}{\gamma_0}\frac{\dot{\chi}}{\cos\chi}\left(\frac{L_y}{\pi\Delta}\right)^2 =\,&\frac{2A}{\mu_0 M_s\Delta^2}\sin\chi \\
&+ \frac{\pi}{2}\frac{D}{\mu_0 M_s\Delta}\sin\phi \\
&- \frac{1}{2}M_s\left(N_y - N_x\right)\sin\left(2(\phi-\chi)\right)\cos\chi
\end{aligned} \tag{A.6}
$$

where L_y is the width of the nanowire.

Equations (A.3) and (A.4) for respectively $\dot{q}$ and $\dot{\phi}$ can be used to derive equations proposed in other collective coordinate models. These are the same equations found in the $q - \phi - \chi$ model [12], while assuming $\chi = 0$ yields the relevant equations of the $q - \phi$ [8] and $q - \phi - \Delta$ [11] models. While equation (A.5) for $\dot{\Delta}$ is identical to the one found in the $q - \phi - \Delta$ model (with $\chi = 0$), equation (A.6) for $\dot{\chi}$ does not match the respective equation in the $q - \phi - \chi$ model. Unlike the $q - \phi - \chi$ model, the evolution of χ in this model is not directly dependent on the magnetocrystalline anisotropy. Instead, it is only indirectly related to this parameter through Δ.

AppendixB. The semi-analytical approach

AppendixB.1. Deriving the equations of motion

Based on averaging the LLG-equation, a semi-analytical model can be developed [16]. To this end, the locally varying effective field (3) is first averaged over the DW volume

$$
\begin{aligned}
\mathbf{H}_{\text{DW}} \equiv\,&\mathbf{H}_{\text{ext}} + \frac{1}{\langle m_{\text{ip}}^2\rangle}\langle\mathbf{H}_{\text{ani}}m_{\text{ip}}^2\rangle + \frac{1}{\langle m_{\text{ip}}^2\rangle}\langle\mathbf{H}_{\text{ms}}m_{\text{ip}}^2\rangle \\
&+ \frac{1}{\zeta_{\text{DMI}}}\langle\mathbf{H}_{\text{DMI}}\rangle + \frac{1}{\zeta_{\text{exch}}}\langle\mathbf{H}_{\text{exch}}\rangle \\
\cong\,&H_{\text{ext},x}\mathbf{e}_x + H_{\text{ext},y}\mathbf{e}_y + H_{\text{ext},z}\mathbf{e}_z + \frac{2K_U}{\mu_0 M_s}\frac{\langle m_z m_{\text{ip}}^2\rangle}{\langle m_{\text{ip}}^2\rangle}\mathbf{e}_z \\
&- \frac{M_s}{\langle m_{\text{ip}}^2\rangle}\left[N_{\text{eff},x}\langle m_x m_{\text{ip}}^2\rangle\mathbf{e}_x + N_{\text{eff},y}\langle m_y m_{\text{ip}}^2\rangle\mathbf{e}_y\right] \\
&- \frac{M_s}{\langle m_{\text{ip}}^2\rangle}N_{\text{eff},z}\langle m_z m_{\text{ip}}^2\rangle\mathbf{e}_z \\
&+ \frac{2D}{\mu_0 M_s\zeta_{\text{DMI}}}\left[\langle\partial_x m_z\rangle\mathbf{e}_x + \langle\partial_y m_z\rangle\mathbf{e}_y\right] \\
&- \frac{2D}{\mu_0 M_s\zeta_{\text{DMI}}}\langle\partial_x m_x + \partial_y m_y\rangle\mathbf{e}_z \\
&+ \frac{2A}{\mu_0 M_s\zeta_{\text{exch}}}\left[\langle\partial_{xx}m_x\rangle\mathbf{e}_x + \langle\partial_{yy}m_y\rangle\mathbf{e}_y + \langle\partial_{zz}m_z\rangle\mathbf{e}_z\right].
\end{aligned} \tag{B.1}
$$

In this expression, $\langle f\rangle$ is a spatial average of the function f over the domain wall volume V_{DW}

$$
\langle f\rangle(t) = \frac{1}{V_{\text{DW}}}\int\int\int_{V_{\text{DW}}}f(\mathbf{r},t)\,\mathrm{d}V \tag{B.2}
$$

as detailed in AppendixE and $\mathbf{m}_{\text{ip}}$ is the in-plane magnetization.

In equation (B.1), the anisotropy field $\mathbf{H}_{\text{ani}}$ and the magnetostatic field $\mathbf{H}_{\text{ms}}$ are multiplied with the weight function $\frac{m_{\text{ip}}^2}{\langle m_{\text{ip}}^2\rangle}$ to confine their averaged contributions to $\mathbf{H}_{\text{DW}}$ to the domain wall.

On the other hand, the averaged DMI and exchange field are scaled with respective factors ζ_{DMI} and ζ_{exch}. We assume these scaling factors are given by

$$
\zeta_{\text{DMI}} = \zeta_{\text{exch}} = \frac{\langle|m_{\text{ip}}|\rangle^2}{\langle m_{\text{ip}}^2\rangle} \tag{B.3}
$$

as earlier determined for DW dynamics in a nanostrip [16]. Note that the DW averaged effective field $\mathbf{H}_{\text{DW}}$ (B.1) is then independent of the denominators in (B.2). Moreover, when limiting the averages to a single discretization cell, $\mathbf{H}_{\text{DW}}$ simplifies to the effective field $\mathbf{H}_{\text{eff}}$ in this cell. We also assumed that $\langle\mathbf{H}_{\text{ms}}m_{\text{ip}}^2\rangle = \langle(-\hat{N}.M_s\mathbf{m})m_{\text{ip}}^2\rangle$ with $\hat{N}$ the local demagnetizing tensor [44], is approximated by

$$
\langle\mathbf{H}_{\text{ms}}m_{\text{ip}}^2\rangle \cong -M_s N_{\text{eff},i}(t)\langle m_i m_{\text{ip}}^2\rangle(t)\,\forall i,j\in\{x,y,z\} \tag{B.4}
$$

with $\hat{N}_{\text{eff}}$ an effective demagnetizing diagonal tensor. To determine the demagnetizing factors from the micromagnetic simulations, we have considered a volume equal to the DW

$$
M_{s,\text{local}}(\mathbf{r}) = |m_{\text{ip}}|_{\text{local}}(\mathbf{r})M_s. \tag{B.5}
$$

11

In this volume, we have determined the demagnetizing factors from the uniform magnetized states as

$$N_{\text{eff},i} = \frac{\langle H_{\text{ms},i} \rangle}{-\langle M_{\text{s,local}} m_i \rangle} = \frac{\langle H_{\text{ms},i} \rangle}{-M_{\text{s}} \langle |m_{\text{ip}}|_{\text{local}} m_i \rangle} \quad \forall i \in \{x, y, z\}. \quad (B.6)$$

The DW position is given by

$$Q(t) = \frac{1}{-\langle \partial_x m_z(\mathbf{r}, t) \rangle} \langle m_z(\mathbf{r}, t) \rangle, \quad (B.7)$$

irrespective of the domain magnetization directions [16]. In the case that there is no DMI (DMI induces edge effects in the domains) and no in-plane fields are applied (in-plane fields induce canting in the domains), equation (B.7) can be simplified to

$$Q(t) = \frac{L_x}{2} \nu \langle m_z(\mathbf{r}, t) \rangle \quad (B.8)$$

with the average $\langle f \rangle$ taken over any volume of the nanostrip including the DW [13–15] and with $\nu = 1$ [$\nu = -1$] if the domain magnetization left of the domain wall has a component along the positive [negative] z-direction.

The DW velocity is then expressed as the derivative of the DW position Q

$$v(t) \equiv \frac{\mathrm{d}Q(t)}{\mathrm{d}t} \cong \frac{1}{-\langle \partial_x m_z(\mathbf{r}, t) \rangle} \frac{\mathrm{d}\langle m_z(\mathbf{r}, t) \rangle}{\mathrm{d}t}$$
$$= \frac{1}{-\langle \partial_x m_z(\mathbf{r}, t) \rangle} \langle \frac{\partial m_z(\mathbf{r}, t)}{\partial t} \rangle, \quad (B.9)$$

using Leibniz' integral rule. To rewrite expression (B.9) as a function of the different interactions with the DW magnetization, equation (B.1) is substituted in the LLG equation (1) and explicitly written and averaged in the z-direction, giving us an expression for $\langle \frac{\partial m_z}{\partial t} \rangle$

$$\langle \frac{\partial m_z}{\partial t} \rangle = \frac{\gamma_0}{1 + \alpha^2} \left[H_{\text{DW},x} \langle m_y \rangle - H_{\text{DW},y} \langle m_x \rangle \right]$$
$$+ \frac{\alpha \gamma_0}{1 + \alpha^2} H_{\text{DW},z} \langle m_{\text{ip}}^2 \rangle$$
$$- \frac{\alpha \gamma_0}{1 + \alpha^2} \left[H_{\text{DW},x} \langle m_x m_z \rangle + H_{\text{DW},y} \langle m_y m_z \rangle \right]$$
$$+ \frac{\beta - \alpha}{1 + \alpha^2} u_x \langle m_x \partial_x m_y - m_y \partial_x m_x \rangle$$
$$+ \frac{1 + \alpha \beta}{1 + \alpha^2} u_x \left[-\langle \partial_x m_z \rangle \right] \quad (B.10)$$

in its most concise form. Similarly, equations for $\langle \frac{\partial m_x}{\partial t} \rangle$ and $\langle \frac{\partial m_y}{\partial t} \rangle$ are derived. By combining equation (B.9) and (B.10), we

have an expression for the DW velocity

$$v = \frac{\langle m_{\text{ip}}^2 \rangle}{-\langle \partial_x m_z \rangle} \frac{\alpha \gamma_0}{1 + \alpha^2} H_{\text{DW},z}$$
$$- \frac{\langle m_{\text{ip}}^2 \rangle}{-\langle \partial_x m_z \rangle} \frac{\alpha \gamma_0}{1 + \alpha^2} \left[H_{\text{DW},x} \frac{\langle m_x m_z \rangle}{\langle m_{\text{ip}}^2 \rangle} + H_{\text{DW},y} \frac{\langle m_y m_z \rangle}{\langle m_{\text{ip}}^2 \rangle} \right]$$
$$+ \frac{\langle m_{\text{ip}}^2 \rangle}{-\langle \partial_x m_z \rangle} \frac{\gamma_0}{1 + \alpha^2} \left[H_{\text{DW},x} \frac{\langle m_y \rangle}{\langle m_{\text{ip}}^2 \rangle} - H_{\text{DW},y} \frac{\langle m_x \rangle}{\langle m_{\text{ip}}^2 \rangle} \right]$$
$$+ \frac{1 + \alpha \beta}{1 + \alpha^2} u_x \quad (B.11)$$
$$+ \frac{\langle m_{\text{ip}}^2 \rangle}{-\langle \partial_x m_z \rangle} \frac{\beta - \alpha}{1 + \alpha^2} u_x \frac{\langle m_x \partial_x m_y - m_y \partial_x m_x \rangle}{\langle m_{\text{ip}}^2 \rangle}.$$

A local in-plane magnetization angle is defined as

$$\phi(\mathbf{r}, t) = \arctan \frac{m_y(\mathbf{r}, t)}{m_x(\mathbf{r}, t)}. \quad (B.12)$$

Taking into account that

$$m_{\text{ip}}^2 \frac{\partial \phi}{\partial t} = m_x \frac{\partial m_y}{\partial t} - m_y \frac{\partial m_x}{\partial t}, \quad (B.13)$$

we also derive a concise expression for the change of magnetization angle inside the DW

$$\frac{1 + \alpha^2}{\gamma_0} \frac{\langle m_{\text{ip}}^2 \frac{\partial \phi}{\partial t} \rangle}{\langle m_{\text{ip}}^2 \rangle} = H_{\text{DW},z}$$
$$- H_{\text{DW},x} \frac{\langle m_x m_z \rangle}{\langle m_{\text{ip}}^2 \rangle} - H_{\text{DW},y} \frac{\langle m_y m_z \rangle}{\langle m_{\text{ip}}^2 \rangle}$$
$$- \alpha \left[H_{\text{DW},x} \frac{\langle m_y \rangle}{\langle m_{\text{ip}}^2 \rangle} - H_{\text{DW},y} \frac{\langle m_x \rangle}{\langle m_{\text{ip}}^2 \rangle} \right]$$
$$+ \frac{\beta - \alpha}{\gamma_0} u_x \left[\frac{-\langle \partial_x m_z \rangle}{\langle m_{\text{ip}}^2 \rangle} \right] \quad (B.14)$$
$$- \frac{1 + \alpha \beta}{\gamma_0} u_x \frac{\langle m_x \partial_x m_y - m_y \partial_x m_x \rangle}{\langle m_{\text{ip}}^2 \rangle}.$$

If we replace $H_{\text{DW},x}$, $H_{\text{DW},y}$ and $H_{\text{DW},z}$ by the individual inter-

12

action contributions from equation (B.1), we get

$$
\begin{aligned}
\frac{1+\alpha^2}{\gamma_0}\frac{\langle m_{\mathrm{ip}}^2 \frac{\partial \phi}{\partial t}\rangle}{\langle m_{\mathrm{ip}}^2\rangle} =\ & H_{\mathrm{ext},z} + \frac{\beta-\alpha}{\gamma_0}u_x\left[\frac{-\langle\partial_x m_z\rangle}{\langle m_{\mathrm{ip}}^2\rangle}\right] \\
& -\frac{1+\alpha\beta}{\gamma_0}u_x\frac{\langle m_x\partial_x m_y - m_y\partial_x m_x\rangle}{\langle m_{\mathrm{ip}}^2\rangle} \\
& -\alpha\left[H_{\mathrm{ext},x}\frac{\langle m_y\rangle}{\langle m_{\mathrm{ip}}^2\rangle} - H_{\mathrm{ext},y}\frac{\langle m_x\rangle}{\langle m_{\mathrm{ip}}^2\rangle}\right] \\
& +\alpha M_s N_{\mathrm{eff},x}\frac{\langle m_x m_{\mathrm{ip}}^2\rangle\langle m_y\rangle}{\langle m_{\mathrm{ip}}^2\rangle^2} \\
& -\alpha M_s N_{\mathrm{eff},y}\frac{\langle m_y m_{\mathrm{ip}}^2\rangle\langle m_x\rangle}{\langle m_{\mathrm{ip}}^2\rangle^2} \\
& -\alpha\frac{2D}{\mu_0 M_s}\left[\frac{\langle\partial_x m_z\rangle\langle m_y\rangle}{\langle|m_{\mathrm{ip}}|\rangle^2} - \frac{\langle\partial_y m_z\rangle\langle m_x\rangle}{\langle|m_{\mathrm{ip}}|\rangle^2}\right] \\
& -\alpha\frac{2A}{\mu_0 M_s}\left[\frac{\langle\partial_{xx}m_x\rangle\langle m_y\rangle}{\langle|m_{\mathrm{ip}}|\rangle^2} - \frac{\langle\partial_{yy}m_y\rangle\langle m_x\rangle}{\langle|m_{\mathrm{ip}}|\rangle^2}\right] \\
& -\left[H_{\mathrm{ext},x}\frac{\langle m_x m_z\rangle}{\langle m_{\mathrm{ip}}^2\rangle} + H_{\mathrm{ext},y}\frac{\langle m_y m_z\rangle}{\langle m_{\mathrm{ip}}^2\rangle}\right] \\
& +\left(\frac{2K_U}{\mu_0 M_s} - M_s N_{\mathrm{eff},z}\right)\frac{\langle m_z m_{\mathrm{ip}}^2\rangle}{\langle m_{\mathrm{ip}}^2\rangle} \\
& + M_s N_{\mathrm{eff},x}\frac{\langle m_x m_{\mathrm{ip}}^2\rangle\langle m_x m_z\rangle}{\langle m_{\mathrm{ip}}^2\rangle^2} \\
& + M_s N_{\mathrm{eff},y}\frac{\langle m_y m_{\mathrm{ip}}^2\rangle\langle m_y m_z\rangle}{\langle m_{\mathrm{ip}}^2\rangle^2} \\
& -\frac{2D}{\mu_0 M_s}\frac{\langle\partial_x m_x + \partial_y m_y\rangle\langle m_{\mathrm{ip}}^2\rangle}{\langle|m_{\mathrm{ip}}|\rangle^2} \\
& -\frac{2D}{\mu_0 M_s}\left[\frac{\langle\partial_x m_z\rangle\langle m_x m_z\rangle}{\langle|m_{\mathrm{ip}}|\rangle^2} + \frac{\langle\partial_y m_z\rangle\langle m_y m_z\rangle}{\langle|m_{\mathrm{ip}}|\rangle^2}\right] \\
& +\frac{2A}{\mu_0 M_s}\frac{\langle\partial_{zz}m_z\rangle\langle m_{\mathrm{ip}}^2\rangle}{\langle|m_{\mathrm{ip}}|\rangle^2} \\
& -\frac{2A}{\mu_0 M_s}\frac{\langle\partial_{xx}m_x\rangle\langle m_x m_z\rangle}{\langle|m_{\mathrm{ip}}|\rangle^2} \\
& -\frac{2A}{\mu_0 M_s}\frac{\langle\partial_{yy}m_y\rangle\langle m_y m_z\rangle}{\langle|m_{\mathrm{ip}}|\rangle^2}.
\end{aligned}
\tag{B.15}
$$

This can be rewritten as

$$
\begin{aligned}
\frac{1+\alpha^2}{\gamma_0}\frac{\langle m_{\mathrm{ip}}^2 \frac{\partial \phi}{\partial t}\rangle}{\langle m_{\mathrm{ip}}^2\rangle} =\ & H_{\mathrm{ext},z} + \frac{\beta-\alpha}{\gamma_0}u_x\left[\frac{-\langle\partial_x m_z\rangle}{\langle m_{\mathrm{ip}}^2\rangle}\right] \\
& -\frac{1+\alpha\beta}{\gamma_0}u_x\frac{\langle m_x\partial_x m_y - m_y\partial_x m_x\rangle}{\langle m_{\mathrm{ip}}^2\rangle} \\
& -\alpha\left[f_{H_{\mathrm{ext},x}} + f_{H_{\mathrm{ext},y}} + f_{\mathrm{ms}} + f_{\mathrm{DMI}} + f_{\mathrm{exch}}\right] \\
& -\left[g_{H_{\mathrm{ext},x}} + g_{H_{\mathrm{ext},y}} + g_{\mathrm{ani}}\right] \\
& -\left[g_{\mathrm{ms}} + g_{\mathrm{DMI}} + g_{\mathrm{exch}}\right],
\end{aligned}
\tag{B.16}
$$

Here, the functions $f_{H_{\mathrm{ext},x}}$, $f_{H_{\mathrm{ext},y}}$, f_{ms}, f_{DMI} and f_{exch} express how the different interactions act on the in-plane DW magnetization and are defined as

$$
\begin{aligned}
f_{H_{\mathrm{ext},x}} =\ & H_{\mathrm{ext},x}\frac{\langle m_y\rangle}{\langle m_{\mathrm{ip}}^2\rangle} \\
f_{H_{\mathrm{ext},y}} =\ & -H_{\mathrm{ext},y}\frac{\langle m_x\rangle}{\langle m_{\mathrm{ip}}^2\rangle} \\
f_{\mathrm{ms}} =\ & M_s\left[N_{\mathrm{eff},y}\frac{\langle m_y m_{\mathrm{ip}}^2\rangle\langle m_x\rangle}{\langle m_{\mathrm{ip}}^2\rangle^2} - N_{\mathrm{eff},x}\frac{\langle m_x m_{\mathrm{ip}}^2\rangle\langle m_y\rangle}{\langle m_{\mathrm{ip}}^2\rangle^2}\right] \\
f_{\mathrm{DMI}} =\ & \frac{2D}{\mu_0 M_s}\left[\frac{\langle\partial_x m_z\rangle\langle m_y\rangle}{\langle|m_{\mathrm{ip}}|\rangle^2} - \frac{\langle\partial_y m_z\rangle\langle m_x\rangle}{\langle|m_{\mathrm{ip}}|\rangle^2}\right] \\
f_{\mathrm{exch}} =\ & \frac{2A}{\mu_0 M_s}\left[\frac{\langle\partial_{xx}m_x\rangle\langle m_y\rangle}{\langle|m_{\mathrm{ip}}|\rangle^2} - \frac{\langle\partial_{yy}m_y\rangle\langle m_x\rangle}{\langle|m_{\mathrm{ip}}|\rangle^2}\right].
\end{aligned}
\tag{B.17}
$$

Moreover, the functions $g_{H_{\mathrm{ext},x}}$, $g_{H_{\mathrm{ext},y}}$, g_{ani}, g_{ms}, g_{DMI} and g_{exch} are defined as

$$
\begin{aligned}
g_{H_{\mathrm{ext},x}} =\ & H_{\mathrm{ext},x}\frac{\langle m_x m_z\rangle}{\langle m_{\mathrm{ip}}^2\rangle} \\
g_{H_{\mathrm{ext},y}} =\ & H_{\mathrm{ext},y}\frac{\langle m_y m_z\rangle}{\langle m_{\mathrm{ip}}^2\rangle} \\
g_{\mathrm{ani}} =\ & -\frac{2K_U}{\mu_0 M_s}\frac{\langle m_z m_{\mathrm{ip}}^2\rangle}{\langle m_{\mathrm{ip}}^2\rangle} \\
g_{\mathrm{ms}} =\ & M_s N_{\mathrm{eff},z}\frac{\langle m_z m_{\mathrm{ip}}^2\rangle}{\langle m_{\mathrm{ip}}^2\rangle} - M_s N_{\mathrm{eff},x}\frac{\langle m_x m_{\mathrm{ip}}^2\rangle\langle m_x m_z\rangle}{\langle m_{\mathrm{ip}}^2\rangle^2} \\
& - M_s N_{\mathrm{eff},y}\frac{\langle m_y m_{\mathrm{ip}}^2\rangle\langle m_y m_z\rangle}{\langle m_{\mathrm{ip}}^2\rangle^2} \\
g_{\mathrm{DMI}} =\ & \frac{2D}{\mu_0 M_s}\frac{\langle\partial_x m_x + \partial_y m_y\rangle\langle m_{\mathrm{ip}}^2\rangle}{\langle|m_{\mathrm{ip}}|\rangle^2} \\
& + \frac{2D}{\mu_0 M_s}\left[\frac{\langle\partial_x m_z\rangle\langle m_x m_z\rangle}{\langle|m_{\mathrm{ip}}|\rangle^2} + \frac{\langle\partial_y m_z\rangle\langle m_y m_z\rangle}{\langle|m_{\mathrm{ip}}|\rangle^2}\right] \\
g_{\mathrm{exch}} =\ & -\frac{2A}{\mu_0 M_s}\frac{\langle\partial_{zz}m_z\rangle\langle m_{\mathrm{ip}}^2\rangle}{\langle|m_{\mathrm{ip}}|\rangle^2} \\
& + \frac{2A}{\mu_0 M_s}\left[\frac{\langle\partial_{xx}m_x\rangle\langle m_x m_z\rangle}{\langle|m_{\mathrm{ip}}|\rangle^2} + \frac{\langle\partial_{yy}m_y\rangle\langle m_y m_z\rangle}{\langle|m_{\mathrm{ip}}|\rangle^2}\right]
\end{aligned}
\tag{B.18}
$$

and are a measure for the DW asymmetry. This is understood as follows: when the DW is symmetric [16], m_z, $\partial_x m_x$ and $\partial_{zz}m_z$ are odd functions while m_x, m_y, $\partial_x m_z$, $\partial_{xx}m_x$ and $\partial_{yy}m_y$ are even functions in the x-direction. Moreover, when the DW is geometrically tilted in a symmetric way, $\partial_y m_y$ is an odd function while $\partial_y m_z$ is an even function in the x-direction. Since integration over an odd function equals 0, we directly deduce that the g-functions can only be non-zero when the DW is not perfectly symmetric.

The definition of these functions enables us to rewrite equa-

13

tion (B.11) concisely as

$$
\begin{aligned}
v = &\frac{\langle m_{\mathrm{ip}}^2 \rangle}{-\langle \partial_x m_z \rangle} \frac{\alpha \gamma_0}{1 + \alpha^2} H_{\mathrm{ext},z} + \frac{1 + \alpha\beta}{1 + \alpha^2} u_x \\
&+ \frac{\langle m_{\mathrm{ip}}^2 \rangle}{-\langle \partial_x m_z \rangle} \frac{\beta - \alpha}{1 + \alpha^2} u_x \frac{\langle m_x \partial_x m_y - m_y \partial_x m_x \rangle}{\langle m_{\mathrm{ip}}^2 \rangle} \\
&+ \frac{\langle m_{\mathrm{ip}}^2 \rangle}{-\langle \partial_x m_z \rangle} \frac{\gamma_0}{1 + \alpha^2} \left[f_{H_{\mathrm{ext},x}} + f_{H_{\mathrm{ext},y}} \right] \\
&+ \frac{\langle m_{\mathrm{ip}}^2 \rangle}{-\langle \partial_x m_z \rangle} \frac{\gamma_0}{1 + \alpha^2} \left[f_{\mathrm{ms}} + f_{\mathrm{DMI}} + f_{\mathrm{exch}} \right] \\
&- \frac{\langle m_{\mathrm{ip}}^2 \rangle}{-\langle \partial_x m_z \rangle} \frac{\alpha \gamma_0}{1 + \alpha^2} \left[g_{H_{\mathrm{ext},x}} + g_{H_{\mathrm{ext},y}} + g_{\mathrm{ani}} \right] \\
&- \frac{\langle m_{\mathrm{ip}}^2 \rangle}{-\langle \partial_x m_z \rangle} \frac{\alpha \gamma_0}{1 + \alpha^2} \left[g_{\mathrm{ms}} + g_{\mathrm{DMI}} + g_{\mathrm{exch}} \right].
\end{aligned}
\tag{B.19}
$$

AppendixB.2. Identification of the DW variables

From equations (B.15) and (B.19), we can identify several DW variables. As discussed in Section 3, the DW motion in Lagrangian-based CCMs is described by maximal 4 DW variables (q, ϕ, Δ and χ). In the semi-analytical model, we identify the analogs for these DW variables as well as additional DW variables.

While the DW position Q is defined by equation (B.7), the DW magnetization angle Φ_{av} is defined as

$$
\begin{aligned}
\tan \Phi_{\mathrm{av}} &= \frac{\langle m_y \rangle}{\langle m_x \rangle} \\
&= \frac{\langle |m_{\mathrm{ip}}| \sin(\phi) \rangle}{\langle |m_{\mathrm{ip}}| \cos(\phi) \rangle}.
\end{aligned}
\tag{B.20}
$$

This way, also the cosine and sine of Φ_{av} are determined by

$$
\begin{cases}
\cos \Phi_{\mathrm{av}} &= \frac{\langle m_x \rangle}{\langle |m_{\mathrm{ip}}| \rangle} \\
\sin \Phi_{\mathrm{av}} &= \frac{\langle m_y \rangle}{\langle |m_{\mathrm{ip}}| \rangle}.
\end{cases}
\tag{B.21}
$$

A weighted DW magnetization angle $\Phi_{\mathrm{av,w}}$ can be defined as

$$
\begin{aligned}
\tan \Phi_{\mathrm{av,w}} &= \frac{\langle m_y m_{\mathrm{ip}}^2 \rangle}{\langle m_x m_{\mathrm{ip}}^2 \rangle} \\
&= \frac{\langle |m_{\mathrm{ip}}|^3 \sin(\phi) \rangle}{\langle |m_{\mathrm{ip}}|^3 \cos(\phi) \rangle}
\end{aligned}
\tag{B.22}
$$

and its cosine and sine are then determined by

$$
\begin{cases}
\cos \Phi_{\mathrm{av,w}} &= \frac{\langle m_x m_{\mathrm{ip}}^2 \rangle}{\langle |m_{\mathrm{ip}}|^3 \rangle} \\
\sin \Phi_{\mathrm{av,w}} &= \frac{\langle m_y m_{\mathrm{ip}}^2 \rangle}{\langle |m_{\mathrm{ip}}|^3 \rangle}.
\end{cases}
\tag{B.23}
$$

To define Φ_{av} unambiguously, we impose that $\Phi_{\mathrm{av}} = 0$ corresponds to a Néel wall characterized by $\langle m_y \rangle = 0$ and $\langle m_x \rangle > 0$ while $\Phi_{\mathrm{av}} = \pi$ corresponds to a Néel wall characterized by $\langle m_y \rangle = 0$ and $\langle m_x \rangle < 0$.

Moreover, the DW width Δ_{av} can be defined as

$$
\Delta_{\mathrm{av}} = -2 \frac{\langle m_{\mathrm{ip}}^2 \rangle}{\langle \partial_x m_z \rangle}.
\tag{B.24}
$$

The DW geometrical tilting angle X_{av} is defined as

$$
\tan X_{\mathrm{av}} = \frac{\langle \partial_y m_z \rangle}{\langle \partial_x m_z \rangle}.
\tag{B.25}
$$

This variable is analogous to the collective coordinate χ introduced by Boulle *et al* [12]. Similar to our earlier model [16], we also define κ_{av} as

$$
\kappa_{\mathrm{av}} = \frac{\langle m_{\mathrm{ip}}^2 \rangle}{\langle |m_{\mathrm{ip}}| \rangle}
\tag{B.26}
$$

which is related to the DW shape, see further, while additionally $\kappa_{\mathrm{av,w}}$ is defined as

$$
\kappa_{\mathrm{av,w}} = \frac{\langle |m_{\mathrm{ip}}|^3 \rangle}{\langle m_{\mathrm{ip}}^2 \rangle}.
\tag{B.27}
$$

We can also define three exchange related DW variables $g_{x,\mathrm{av}}$, $g_{y,\mathrm{av}}$ and $g_{z,\mathrm{av}}$ with

$$
g_{i,\mathrm{av}} = \frac{\langle \partial_{ii} m_i \rangle}{\langle |m_{\mathrm{ip}}| \rangle} \quad \forall i \in \{x, y, z\}.
\tag{B.28}
$$

AppendixB.3. Updated equations of motion

After introducing the DMI-field $H_{\mathrm{DMI}} = \frac{D}{\mu_0 M_{\mathrm{s}} \Delta_{\mathrm{av}}}$ and the exchange field $H_{\mathrm{exch}} = \frac{A}{\mu_0 M_{\mathrm{s}} \Delta_{\mathrm{av}}^2}$, we can use the expressions of the DW variables to rewrite equation (B.15) as

$$
\begin{aligned}
\frac{1 + \alpha^2}{\gamma_0} \frac{\langle m_{\mathrm{ip}}^2 \frac{\partial \phi}{\partial t} \rangle}{\langle m_{\mathrm{ip}}^2 \rangle} = &\ H_{\mathrm{ext},z} + \frac{2}{\Delta_{\mathrm{av}}} \frac{\beta - \alpha}{\gamma_0} u_x \\
&- \frac{\alpha}{\kappa_{\mathrm{av}}} \left[H_{\mathrm{ext},x} \sin \Phi_{\mathrm{av}} - H_{\mathrm{ext},y} \cos \Phi_{\mathrm{av}} \right] \\
&- \alpha M_{\mathrm{s}} \frac{\kappa_{\mathrm{av,w}}}{\kappa_{\mathrm{av}}} N_{\mathrm{eff},y} \sin \Phi_{\mathrm{av,w}} \cos \Phi_{\mathrm{av}} \\
&+ \alpha M_{\mathrm{s}} \frac{\kappa_{\mathrm{av,w}}}{\kappa_{\mathrm{av}}} N_{\mathrm{eff},x} \cos \Phi_{\mathrm{av,w}} \sin \Phi_{\mathrm{av}} \\
&+ \alpha 4 \kappa_{\mathrm{av}} H_{\mathrm{DMI}} \left[\sin \Phi_{\mathrm{av}} - \tan X_{\mathrm{av}} \cos \Phi_{\mathrm{av}} \right] \\
&- \alpha H_{\mathrm{exch}} \left[2\Delta_{\mathrm{av}}^2 \left(g_{x,\mathrm{av}} \sin \Phi_{\mathrm{av}} - g_{y,\mathrm{av}} \cos \Phi_{\mathrm{av}} \right) \right] \\
&+ O_{H_{\mathrm{ext},z}}(\text{asymmetric}),
\end{aligned}
\tag{B.29}
$$

with the asymmetric contributions represented by $O_{H_{\mathrm{ext},z}}(\text{asymmetric})$

$$
\begin{aligned}
O_{H_{\mathrm{ext},z}}(\text{asymmetric}) = &- \frac{1 + \alpha\beta}{\gamma_0} u_x \frac{\langle m_x \partial_x m_y - m_y \partial_x m_x \rangle}{\langle m_{\mathrm{ip}}^2 \rangle} \\
&- \left[g_{H_{\mathrm{ext},x}} + g_{H_{\mathrm{ext},y}} + g_{\mathrm{ani}} \right] \\
&- \left[g_{\mathrm{ms}} + g_{\mathrm{DMI}} + g_{\mathrm{exch}} \right].
\end{aligned}
\tag{B.30}
$$

14

Similarly, we can rewrite equation (B.19) as

$$
\begin{aligned}
\frac{1+\alpha^2}{\gamma_0}\frac{2}{\Delta_{av}}v =& \alpha H_{ext,z} + \frac{2}{\Delta_{av}}\frac{1+\alpha\beta}{\gamma_0}u_x \\
&+ \frac{1}{\kappa_{av}}\left[H_{ext,x}\sin\Phi_{av} - H_{ext,y}\cos\Phi_{av}\right] \\
&+ M_s\frac{\kappa_{av,w}}{\kappa_{av}}N_{eff,y}\sin\Phi_{av,w}\cos\Phi_{av} \\
&- M_s\frac{\kappa_{av,w}}{\kappa_{av}}N_{eff,x}\cos\Phi_{av,w}\sin\Phi_{av} \\
&- 4\kappa_{av}H_{DMI}\left[\sin\Phi_{av} - \tan X_{av}\cos\Phi_{av}\right] \\
&+ H_{exch}\left[2\Delta_{av}^2\left(g_{x,av}\sin\Phi_{av} - g_{y,av}\cos\Phi_{av}\right)\right] \\
&+ \frac{1+\alpha^2}{\gamma_0}\frac{2}{\Delta_{av}}O_{v,1}(\text{asymmetric}) \qquad (B.31)
\end{aligned}
$$

with the asymmetric contributions to the DW velocity expression represented by $O_{v,1}(\text{asymmetric})$

$$
\begin{aligned}
O_{v,1}(\text{asymmetric}) =& \frac{\Delta_{av}}{2}\frac{\beta-\alpha}{1+\alpha^2}u_x\frac{\langle m_x\partial_x m_y - m_y\partial_x m_x\rangle}{\langle m_{ip}^2\rangle} \\
&- \frac{\Delta_{av}}{2}\frac{\alpha\gamma_0}{1+\alpha^2}\left[g_{H_{ext,x}} + g_{H_{ext,y}} + g_{ani}\right] \\
&- \frac{\Delta_{av}}{2}\frac{\alpha\gamma_0}{1+\alpha^2}\left[g_{ms} + g_{DMI} + g_{exch}\right].
\end{aligned}
$$
$$(B.32)$$

Expressions (B.29), (B.30), (B.31) and (B.32) can be combined to

$$
\begin{aligned}
v + \frac{\Delta_{av}}{2}\frac{1}{\alpha}\frac{\langle m_{ip}^2\frac{\partial\phi}{\partial t}\rangle}{\langle m_{ip}^2\rangle} =& \frac{\Delta_{av}}{2}\frac{\gamma_0}{\alpha}H_{ext,z} + \frac{\beta}{\alpha}u_x \\
&+ O_{v,2}(\text{asymmetric}) \qquad (B.33)
\end{aligned}
$$

with $O_{v,2}(\text{asymmetric})$ representing the asymmetric contributions to the DW velocity

$$
\begin{aligned}
O_{v,2}(\text{asymmetric}) =& -\frac{\Delta_{av}}{2}\frac{1}{\alpha}u_x\frac{\langle m_x\partial_x m_y - m_y\partial_x m_x\rangle}{\langle m_{ip}^2\rangle} \\
&- \frac{\Delta_{av}}{2}\frac{\gamma_0}{\alpha}\left[g_{H_{ext,x}} + g_{H_{ext,y}} + g_{ani}\right] \\
&- \frac{\Delta_{av}}{2}\frac{\gamma_0}{\alpha}\left[g_{ms} + g_{DMI} + g_{exch}\right].
\end{aligned}
$$
$$(B.34)$$

Since the semi-analytical model contains more unknown variables than equations of motion, we rely on micromagnetic simulations to determine their value.

AppendixC. The DW profile and DW variable κ_{av}

In this Appendix, we demonstrate how to give a physical interpretation to the prefactors κ_{DMI} and κ_{field} from the Lagrangian-based approach and κ_{av} from the semi-analytical model. While κ_{DMI} and κ_{field} are constants in the Lagrangian-based CCMs, κ_{av} defined by

$$
\kappa_{av} = \frac{\langle m_{ip}^2\rangle}{\langle|m_{ip}|\rangle} \qquad (C.1)
$$

is a DW variable. Since expressions $0 \le m_{ip}^2 \le 1$ and $m_{ip}^2 \le |m_{ip}|$ are always valid, κ_{av} is a value between 0 and 1. Note that κ_{DMI} and κ_{field} are also values between 0 and 1. The averages $\langle f\rangle$ can be taken over any volume of the nanostrip including the DW

$$
\langle f\rangle(t) = \frac{1}{V}\int\int\int_V f(\mathbf{r}, t)\,dV \qquad (C.2)
$$

when edge effects due to DMI and magnetization canting of the domains due to in-plane fields are not present. Indeed, when $m_z^2 = 1$ in the domains, $\langle m_{ip}^2\rangle$ and $\langle|m_{ip}|\rangle$ from equation (C.1) will have no contributions from outside the DW. On the other hand, when $m_z^2 < 1$ in the domains, this should be taken into account when integrating over the DW profile. Next, we will use a simplified version of the DW width definition (B.24)

$$
\begin{aligned}
\Delta_{av} &= L_x\langle m_{ip}^2\rangle \qquad (C.3) \\
&= \frac{L_x}{V}\int\int\int_V 1 - m_z^2(\mathbf{r}, t)\,dV \\
&= \frac{1}{L_y}\int_{-\frac{L_y}{2}}^{\frac{L_y}{2}}\int_{-\frac{L_x}{2}}^{\frac{L_x}{2}} 1 - m_z^2(x, y, t)\,dxdy.
\end{aligned}
$$

to determine κ_{av} and to ensure that the boundary conditions of the DW profile are well defined. L_x, L_y and L_z are respectively the length, the width and the thickness of the integrated nanostrip volume.

To understand what κ_{av} represents, we consider the different cases illustrated in Figure C.6.

In the first case, we consider the hypothetical DW profile depicted in the left part of Fig. C.6. This DW has only an in-plane magnetized contribution, i.e.

$$
m_z(x) = 0 \text{ when } q - \frac{\Delta_{av}}{2} \le x \le q + \frac{\Delta_{av}}{2}. \qquad (C.4)
$$

Consequently, m_{ip}^2 and $|m_{ip}|$ are both equal to 1 in every point of the DW. This corresponds to $\kappa_{av} = 1$ in accordance with equation (C.1). The edges of this DW profile are at $x = q - \frac{\Delta_{av}}{2}$ and $x = q + \frac{\Delta_{av}}{2}$ to assure the consistency of equation (C.3).

In the second case, we start directly from the ansatz (5) of the DW profile, taking into account that the normalized magnetization vector $\mathbf{m}$ is expressed by (4). In this case, the DW shape is characterized by

$$
\begin{aligned}
m_z(x) &= \cos\left(2\arctan\left[\exp\left(2\frac{(x-q) + y\tan\chi}{\Delta_{av}}\right)\right]\right) \\
&= -\tanh\left(2\frac{(x-q) + y\tan\chi}{\Delta_{av}}\right) \qquad (C.5)
\end{aligned}
$$

in which $\Delta/\cos\chi$ was replaced by $\Delta_{av}/2$ in accordance with Table 1. This DW profile at $y = 0$ is depicted in the right part of Fig. C.6.

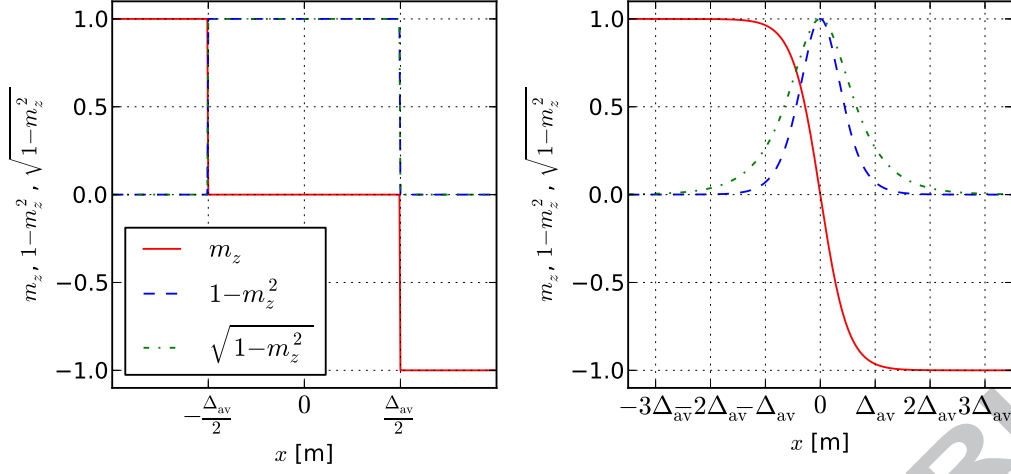Using equations (C.1), (C.2), (C.5) and (C.3) we evaluate κ_{av}

Figure C.6: Comparison of different DW profiles to illustrate how κ_{av} can be interpreted. The left part corresponds to DW profile (C.4) with $q = 0$, while the right part corresponds to DW profile (C.5) at the middle of the nanostrip ($y = 0$) and with $q = 0$. When $\chi = 0$, these DW profiles are also valid at every cross section of the nanostrip, i.e. $\forall y \in [-L_y/2, L_y/2]$.

as

$$
\begin{aligned}
\kappa_{av} &= \frac{\left\langle \frac{1}{\cosh^2\left(2\frac{(x-q)+y\tan\chi}{\Delta_{av}}\right)} \right\rangle}{\left\langle \sqrt{\frac{1}{\cosh^2\left(2\frac{(x-q)+y\tan\chi}{\Delta_{av}}\right)}} \right\rangle} \\
&= \frac{\frac{\Delta_{av}}{L_x}}{\frac{1}{L_x L_y} \int_{-\frac{L_y}{2}}^{\frac{L_y}{2}} \int_{-\infty}^{\infty} \frac{1}{\cosh\left(2\frac{(x-q)+y\tan\chi}{\Delta_{av}}\right)} \, dx dy} \\
&= \frac{\Delta_{av}}{\frac{\Delta_{av}}{2L_y} \int_{-\frac{L_y}{2}}^{\frac{L_y}{2}} \int_{-\infty}^{\infty} \frac{1}{\cosh u} \, du dy} \\
&= \frac{2}{\pi} \approx 0.63662.
\end{aligned}
\tag{C.6}
$$

This is in agreement with the constant κ_{field} in the Lagrangian-based CCMs. However, the constant κ_{DMI} is equal to $\frac{\pi}{4}$. From this discussion, it is clear that κ_{av} is determined by the DW shape.

AppendixD. Assessment of the semi-analytical model

AppendixD.1. Introduction

To make an assessment of the semi-analytical model, we applied the model for both field-driven DW dynamics in Pt/CoFe/MgO nanostrips and STT-driven DW dynamics in Pt/Co/AlO$_x$ nanostrips as detailed in Subsection 5.2. Micromagnetic simulations enable us to quantify the DW variables and to use the semi-analytical equations to predict the DW velocity and the excitation strength. The accuracy of these predictions can then be determined since the DW velocity can also be extracted from the built-in simulation window velocity of MuMax[3] which gives the speed of the simulation window. Moreover, we can verify how well the DW variables defined

in AppendixB correspond to their analogs in the Lagrangian-based CCMs by extracting them from simulations. These analogs were extracted using following methods:

- The in-plane magnetization angle ϕ was extracted from the local values of the x-and y-component of magnetization at the center of the DW (position q corresponding to $m_z = 0$ and $y = 0$) in accordance with the definition used for deriving the Lagrangian-based CCMs as depicted in Fig. 1.

- The tilting angle χ was extracted by finding the position of the DW at the edges of the nanostrip, and computing the angle of the line connecting the two points with respect to the width of the nanostrip through the center of the DW (q), i.e. the tilting angle of the line $m_z = 0$ with respect to the y-direction as depicted in Fig. 1.

- The DW width was extracted based on the Thiele definition of DW width [11, 46]

$$
\Delta \equiv \frac{2L_y L_z}{\int \int \int_V \left(\frac{\partial \mathbf{m}}{\partial x}\right)^2 dV}
\tag{D.1}
$$

This DW width Δ corresponds to $\Delta / \cos\chi$ in Table 1.

Additionally, to investigate how much edge effects affect the DW dynamics, we also quantified the semi-analytical DW variables by averaging the DW profile over the line along the length of the nanostrip and through the middle of the nanostrip cross section, i.e. the line characterized by $y = 0$ in Fig. 1(b). These DW variables are also substituted in the semi-analytical equations of motion to investigate how strongly the edge effects affect their evaluation.

Furthermore, the effective demagnetizing factors determined from micromagnetic simulations as explained in AppendixB

16

are compared to the demagnetizing factors calculated using Aharoni's equations [38]. While $N_{\text{eff},z}$ is not depicted for clarity, $N_{\text{eff},z}$ is determined by the other two demagnetizing factors ($N_{\text{eff},z} = 1 - N_{\text{eff},x} - N_{\text{eff},y}$).

In general, one can discriminate between two propagation regimes, separated by the Walker Breakdown (WB) [43]. Below the WB, the DW adapts itself to the perpendicularly applied field or the applied current along the length of the nanostrip, resulting in a steady state translational motion along the nanostrip. In the equations of motion, this corresponds to

$$\langle m_{\text{ip}}^2 \frac{\partial \phi}{\partial t} \rangle = 0, \tag{D.2}$$

i.e. a fixed magnetization profile. Under these conditions, the left hand side of equation (B.16) is zero and thus

$$\alpha \left[f_{\text{ms}} + f_{\text{DMI}} + f_{H_{\text{ext},x}} + f_{H_{\text{ext},y}} + f_{\text{exch}} \right]$$
$$+ \left[g_{H_{\text{ext},x}} + g_{H_{\text{ext},y}} + g_{\text{ani}} + g_{\text{ms}} + g_{\text{DMI}} + g_{\text{exch}} \right]$$
$$= H_{\text{ext},z} \tag{D.3}$$

for the field-driven case and

$$\frac{\alpha \zeta}{-b_J} \left[f_{\text{ms}} + f_{\text{DMI}} + f_{H_{\text{ext},x}} + f_{H_{\text{ext},y}} + f_{\text{exch}} \right]$$
$$+ \frac{\zeta}{-b_J} \left[g_{H_{\text{ext},x}} + g_{H_{\text{ext},y}} + g_{\text{ani}} + g_{\text{ms}} + g_{\text{DMI}} + g_{\text{exch}} \right]$$
$$= j_x \tag{D.4}$$

with

$$\zeta = \frac{\gamma_0}{\frac{2}{\Delta_{\text{av}}}(\beta - \alpha) - (1 + \alpha\beta)\frac{\langle m_x \partial_x m_y - m_y \partial_x m_x \rangle}{\langle m_{\text{ip}}^2 \rangle}} \tag{D.5}$$

and $-b_J j_x = u_x$ for the STT-driven case. These expressions show how the different symmetric interactions (f-functions on the left hand side) and the asymmetric interactions (g-functions on the left hand side) add up to balance the driving force (right hand side). As long as these interactions can balance $H_{\text{ext},z}$ and/or j_x, the DW motion stays below the WB. The assessment of the semi-analytical model is limited to the DW motion below the WB.

AppendixD.2. Field-driven DW motion

First, we limit our discussion to field-driven DW motion below the WB in Pt/CoFe/MgO nanostrips. From Fig. D.7, it is clear that the magnetization angles Φ_{av} and $\Phi_{\text{av,w}}$ as defined by respective equations (B.20) and (B.22) indeed represent the DW magnetization angle. Similarly, the geometrical tilting angle X_{av} defined by (B.25) represents the DW tilting angle and $\frac{\Delta_{\text{av}}}{2}$ defined by (B.24) corresponds to the Lagrangian-based DW width. Note that, while the DW width curves do not perfectly match, they have the same shape. The difference between the semi-analytical DW variables quantified by averaging over respectively the entire DW profile and the DW profile along the line $y = 0$, demonstrates that the influence of edge effects on the DW variables is rather small.

To verify the accuracy of the derived equations of motion of the semi-analytical model, the DW velocity predicted by equation (B.33) is compared to the DW velocity determined by the built-in simulation window velocity of MuMax[3] for several out-of-plane fields below the Walker Breakdown. This comparison is illustrated in Figure D.8. Moreover, we also verified whether the sum of the terms on the left hand side of equation (D.3) equals $H_{\text{ext},z}$. We also calculated the normalized root mean square error (NRMSE) and coefficient of determination R^2 for this comparison in Table D.5. We can conclude that the semi-analytical approach is very accurate in its predictions. Only at fields close to the Walker Breakdown field, we observe a small deviation: the DW velocity is slightly underestimated, while the out-of-plane field is a little bit overestimated. We also observe that the evaluation of the equations of motion is only slightly affected when edge effects are not taken into account ($y = 0$) and when the demagnetizing factors are calculated using Aharoni's equations [38] instead of determining them from micromagnetic simulations. The effective demagnetizing factors are of the same order of magnitude as those determined by Aharoni's equations, but vary due to the changing DW shape as function of excitation strength.

From Figure D.8, it is clear that the g-functions which are an indication for the DW asymmetry are relatively small compared to the f-functions. Moreover, the DW becomes increasingly asymmetric for larger out-of-plane fields. We also observe that g_{DMI} and f_{DMI} clearly dominate over the other g- and f-functions, respectively. Note that, while asymmetry in the DW slightly slows the DW down, it hereby increases the Walker Breakdown.

AppendixD.3. STT-driven DW motion

For STT-driven DW motion below the WB in Pt/Co/AlO$_x$ nanostrips, the discussion is similar. In Fig. D.9, we observe that the DW variables in the semi-analytical model are well defined.

In Fig. D.10, the DW velocity predicted by equation (B.33) is compared to the DW velocity determined by the built-in simulation window velocity of MuMax[3] for several current densities below the Walker Breakdown. Moreover, we also verified whether the sum of the terms on the left hand side of equation (D.4) equals j_x. We also calculated the normalized root mean square error (NRMSE) and coefficient of determination R^2 for this comparison in Table D.5. We may again conclude that the semi-analytical approach is very accurate in its predictions, both with and without ($y = 0$) taking edge effects into account and when the demagnetizing factors are calculated using Aharoni's equations [38] instead of determining them from micromagnetic simulations. However, at currents close to the Walker Breakdown, the current density is a little bit underestimated.

From Fig. D.10, it is clear that the asymmetric contributions to the DW velocity and to the current density are negligible. This is in contrast to the field-driven case, where asymmetric effects have a significant effect on the DW dynamics. Similar to the field-driven case, we observe that f_{DMI} clearly dominates over the other f-functions.
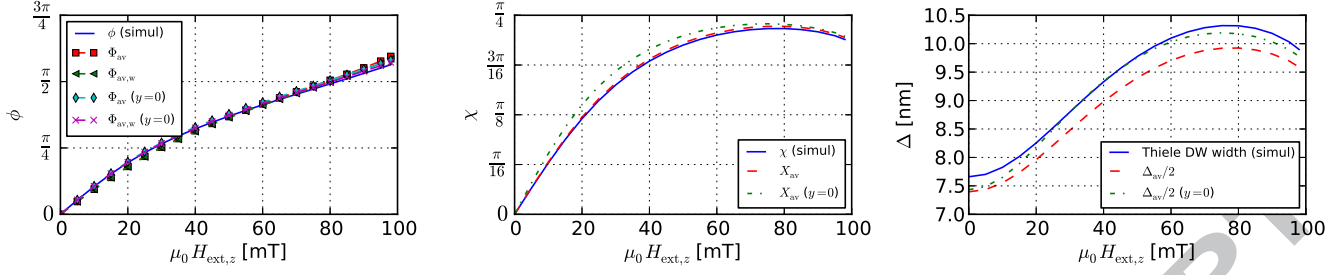
Figure D.7: For field-driven DW motion in a Pt/CoFe/MgO nanostrip, it is shown how well the main DW variables defined in AppendixB correspond to their analogs in the Lagrangian-based CCMs (listed in Table 1), which are determined by extraction from simulations. These semi-analytical DW variables are both determined by averaging over the entire DW and over the line through the middle of the DW ($y = 0$). *From left to right:* the in-plane magnetization angles Φ_{av} (B.20), $\Phi_{av,w}$ (B.22) and their analog ϕ, the geometrical tilting angle X_{av} (B.25) and its analog χ, the scaled DW width $\frac{\Delta_{av}}{2}$ (see eq. (B.24)) and its analog Δ (Thiele definition).
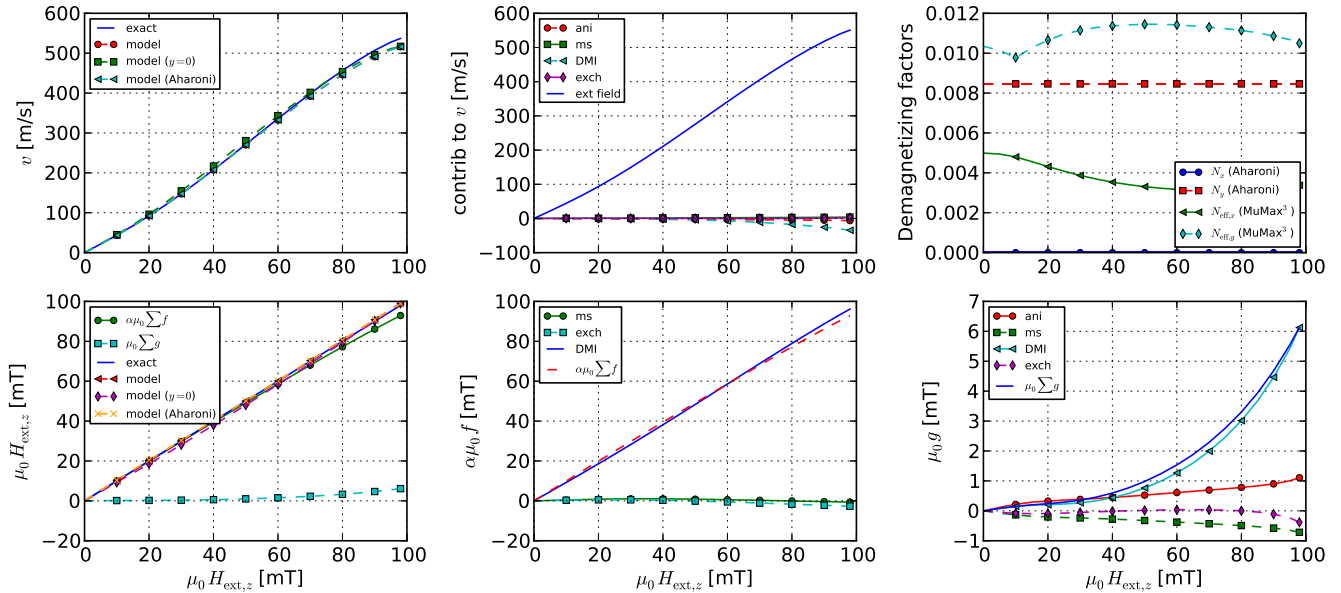

Figure D.8: For field-driven DW motion in a Pt/CoFe/MgO nanostrip, the accuracy of the semi-analytical equations for the DW velocity and the change in magnetization angle is investigated. *Top:* the DW velocity predicted by equation (B.33) (both with and without ($y = 0$) taking edge effects into account, and when using demagnetizing factors calculated with Aharoni's equations [38] instead of determining them from micromagnetic simulations) is compared to the DW velocity determined by the built-in simulation window velocity of MuMax[3] (*left*). The different contributions to this DW velocity according to the interaction (current, anisotropy, magnetostatics, DMI and exchange) are also shown (*middle*). Only the out-of-plane field is a symmetric term while the other interactions are due to asymmetric effects. The micromagnetically determined effective demagnetizing factors $N_{eff,x}$ and $N_{eff,y}$ are also compared to the demagnetizing factors N_x and N_y calculated using Aharoni's equations [38](*right*). *Bottom:* $\mu_0 H_{ext,z}$ as predicted by the left hand side of equation (D.3) (both with and without ($y = 0$) taking edge effects into account, and when using demagnetizing factors calculated with Aharoni's equations [38] instead of determining them from micromagnetic simulations) as well as the combined contributions of the symmetric f-functions and the asymmetric g-functions are compared to the exact value of $\mu_0 H_{ext,z}$ (*left*). The different symmetric contributions (f-functions) (*middle*) and the different asymmetric contributions (g-functions) (*right*) are also shown.

18

Model	Velocity NRMSE [R^2]	Φ_{av} and $\Phi_{av,w}$ with ϕ NRMSE [R^2]		X_{av} with χ NRMSE [R^2]	$\Delta_{av}/2$ with Δ NRMSE [R^2]	$\mu_0 H_{ext,z}$ or j_x NRMSE [R^2]
Pt/CoFe/MgO (field-driven)	3.07% [99.77%]	Φ_{av}	3.99% [99.31%]	1.36% [99.89%]	3.69% [86.76%]	0.84% [99.98%]
		$\Phi_{av,w}$	3.28% [99.53%]			
Pt/Co/AlO$_x$ (STT-driven)	0.64% [99.99%]	Φ_{av}	2.08% [99.82%]	1.35% [99.9%]	3.38% [78.12%]	2.96% [99.75%]
		$\Phi_{av,w}$	2.34% [99.77%]			

Table D.5: The normalized root mean square error (NRMSE) and coefficient of determination R^2 of the DW variables from the semi-analytical model as compared to their analogs from the Lagrangian-based CCMs, which are determined by extraction from simulations, as well as the NRMSE and R^2 of the predictions from this model as compared to the exact values. Both the results for field-driven DW motion in Pt/CoFe/MgO nanostrips and STT-driven DW motion in Pt/Co/AlO$_x$ nanostrips are listed. More specifically, this Table compares the DW velocity predicted by (B.33) with the built-in simulation window velocity of MuMax[3], the in-plane magnetization angles Φ_{av} (B.20) and $\Phi_{av,w}$ (B.22) with their analog ϕ, the tilting angle X_{av} (B.25) with its analog χ, the scaled DW width $\Delta_{av}/2$ (see eq. (B.24)) with the Thiele DW width Δ and the out-of-plane field or current density as determined by (D.3) or (D.4) with the exact out-of-plane field $\mu_0 H_{ext,z}$ or exact current density j_x.
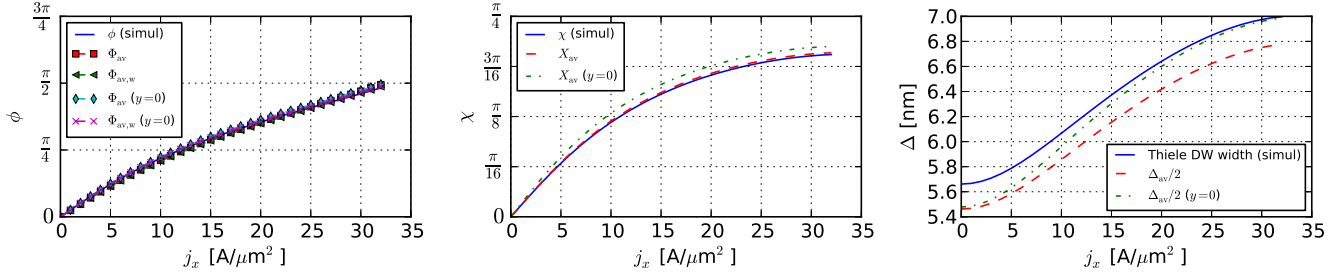

Figure D.9: For STT-driven DW motion in a Pt/Co/AlO$_x$ nanostrip, it is shown how well the main DW variables defined in AppendixB correspond to their analogs in the Lagrangian-based CCMs (listed in Table 1), which are determined by extraction from simulations. These semi-analytical DW variables are both determined by averaging over the entire DW and over the line through the middle of the DW ($y = 0$). *From left to right:* the in-plane magnetization angles Φ_{av} (B.20), $\Phi_{av,w}$ (B.22) and their analog ϕ, the geometrical tilting angle X_{av} (B.25) and its analog χ, the scaled DW width $\frac{\Delta_{av}}{2}$ (see eq. (B.24)) and its analog Δ (Thiele definition).
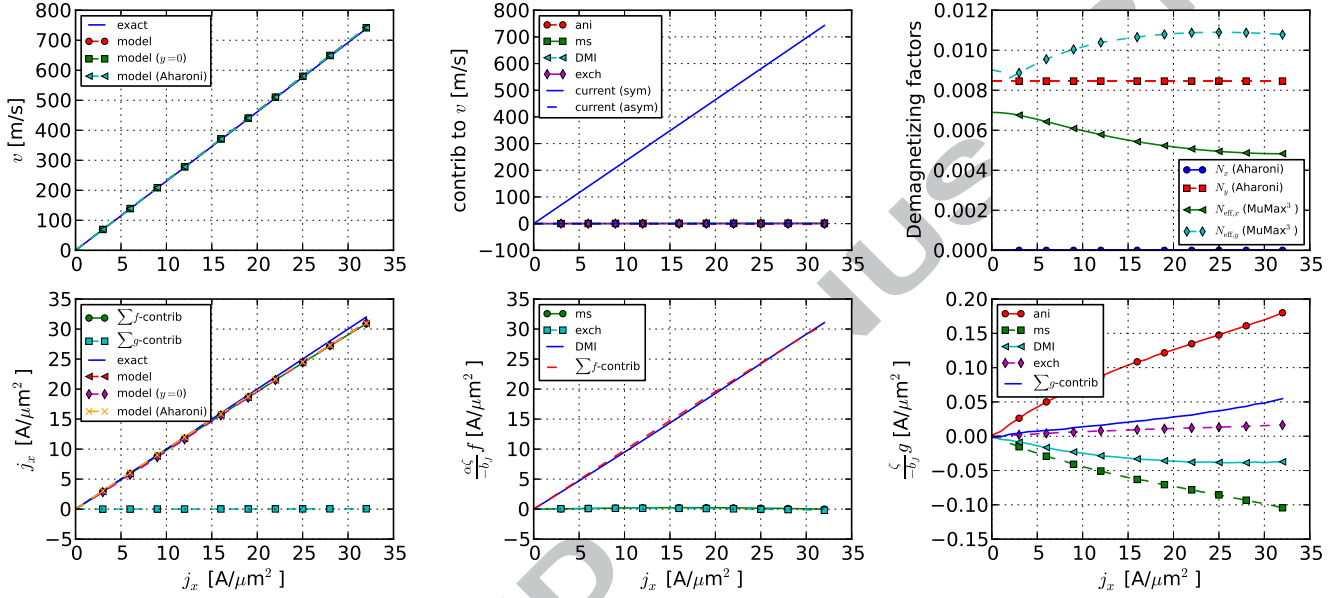
Figure D.10: For STT-driven DW motion in a Pt/Co/AlO$_x$ nanostrip, the accuracy of the semi-analytical equations for the DW velocity and the change in magnetization angle is investigated. *Top:* the DW velocity predicted by equation (B.33) (both with and without ($y = 0$) taking edge effects into account, and when using demagnetizing factors calculated with Aharoni's equations [38] instead of determining them from micromagnetic simulations) is compared to the DW velocity determined by the built-in simulation window velocity of MuMax[3] (*left*). The different contributions to this DW velocity according to the interaction (current, anisotropy, magnetostatics, DMI and exchange) are also shown (*middle*). Only one term due to the current is a symmetric term while the other interactions and another current term are due to asymmetric effects. The micromagnetically determined effective demagnetizing factors $N_{\text{eff},x}$ and $N_{\text{eff},y}$ are also compared to the demagnetizing factors N_x and N_y calculated using Aharoni's equations [38](*right*). *Bottom:* j_x as predicted by the left hand side of equation (D.4) (both with and without ($y = 0$) taking edge effects into account, and when using demagnetizing factors calculated with Aharoni's equations [38] instead of determining them from micromagnetic simulations) as well as the combined contributions of the symmetric f-functions and the asymmetric g-functions are compared to the exact value of j_x (*left*). The different symmetric contributions (f-functions) (*middle*) and the different asymmetric contributions (g-functions) (*right*) are also shown.

AppendixE. Defining the averaging window

In order to accurately describe the DW behaviour using the semi-analytical model, the averages $\langle f \rangle$ have to be calculated in a proper way. In perpendicularly magnetized nanostrips without DMI and in-plane fields, the domain magnetization has no in-plane contributions [16]. The DW position Q is then expressed as [45]

$$Q(t) = \frac{L_x}{2}\langle m_z(\mathbf{r}, t)\rangle \tag{E.1}$$

with the average $\langle f \rangle$ taken over any volume of the nanostrip including the DW [13–15]. Taking into account that DMI induces edge effects and in-plane fields lead to magnetization canting of the domains, eq. (E.1) is replaced by

$$Q(t) = \frac{1}{-\langle \partial_x m_z(\mathbf{r}, t)\rangle}\langle m_z(\mathbf{r}, t)\rangle. \tag{E.2}$$

While the DW position Q is well defined by (E.2) for every averaging window that includes the DW, both effects undesirably affect the evaluation of the equations of motion when a significant part of the domains is taken into account. For example, when $\langle f \rangle$ takes a significant part of the domains into account, the DW width Δ_{av} defined as

$$\Delta_{\mathrm{av}} = 2\frac{\langle m_{\mathrm{ip}}^2\rangle}{-\langle \partial_x m_z\rangle} \tag{E.3}$$

is overestimated and the DW magnetization angle Φ_{av}

$$\tan \Phi_{\mathrm{av}} = \frac{\langle m_y\rangle}{\langle m_x\rangle}, \tag{E.4}$$

is poorly defined. To avoid this, $\langle f \rangle$ is by definition restricted to the DW volume V_{DW}

$$\langle f \rangle(t) = \frac{1}{V_{\mathrm{DW}}}\int\int\int_{V_{\mathrm{DW}}} f(\mathbf{r}, t)\,\mathrm{d}V. \tag{E.5}$$

In order to define the DW volume V_{DW} in (E.5), we fix the boundaries based on m_z changing only significantly inside the DW as a function of x. Therefore, the DW is defined in the region where

$$|\partial_x m_z| \geq \epsilon\,[\mathrm{nm}^{-1}] \tag{E.6}$$

is fulfilled. In equation (E.6), ϵ should be a well-chosen constant. If ϵ is too large, only a small part of the DW is taken into account, thereby neglecting the full complexity of the DW. On the other hand, if ϵ is too small, a significant part of the domains is taken into account causing unwanted contributions to the averages. We found that $\epsilon = 0.01$ results in an accurate description of the DW dynamics by the semi-analytical equations of motion. This value is used consistently in this paper.

Every timestep, the averaging window is redefined and the averages are computed with high precision using interpolation to minimize discretization effects.

[1] D. A. Allwood, G. Xiong, C. C. Faulkner, D. Atkinson, D. Petit, and R. P. Cowburn, Science **309**, 1688 (2005).
[2] K. A. Omari and T. J. Hayward, Phys. Rev. Applied **2**, 044001 (2014).
[3] J. Vandermeulen, B. Van de Wiele, L. Dupré, and B. Van Waeyenberge, J. Phys. D: Appl. Phys. **48**, 275003 (2015).
[4] S. S. P. Parkin, M. Hayashi, and L. Thomas, Science **320**, 190 (2008).
[5] S. S. P. Parkin and S.-H. Yang, Nat. Nanotechnol. **10**, 195 (2015).
[6] K.-W. Moon, D.-H. Kim, S.-C. Yoo, S.-G. Je, B. S. Chun, W. Kim, B.-C. Min, C. Hwang, and S.-B. Choe, Sci. Rep. **5**, 9166 (2015).
[7] J. A. Katine and E. E. Fullerton, J. Magn. Magn. Mater. **320**, 1217 (2008).
[8] J. C. Slonczewski, AIP Conf. Proc. **5**, 170 (1972).
[9] A. Thiaville, Y. Nakatani, J. Miltat, and N. Vernier, J. Appl. Phys. **95**, 7049 (2004).
[10] A. Thiaville, Y. Nakatani, J. Miltat, and Y. Suzuki, Europhys. Lett. **69**, 990 (2005).
[11] A. Thiaville and Y. Nakatani, *Spin Dynamics in Confined Magnetic Structures III* (Springer, Berlin–Heidelberg, 2006), vol. Volume 101/2006 of *Topics Appl. Phys.*, chap. Domain-Wall Dynamics in Nanowires and Nanostrips, pp. 161–205.
[12] O. Boulle, S. Rohart, L. D. Buda-Prejbeanu, E. Jué, I. M. Miron, S. Pizzini, J. Vogel, G. Gaudin, and A. Thiaville, Phys. Rev. Lett. **111**, 217203 (2013).
[13] J. Vandermeulen, B. Van de Wiele, A. Vansteenkiste, B. Van Waeyenberge, and L. Dupré, J. Phys. D: Appl. Phys. **48**, 035001 (2015).
[14] J. Leliaert, B. Van de Wiele, J. Vandermeulen, A. Coene, A. Vansteenkiste, L. Laurson, G. Durin, B. Van Waeyenberge, and L. Dupré, Appl. Phys. Lett. **106**, 202401 (2015).
[15] J. Leliaert, B. Van de Wiele, A. Vansteenkiste, L. Laurson, G. Durin, L. Dupré, and B. Van Waeyenberge, Sci. Rep. **6**, 20472 (2016).
[16] J. Vandermeulen, S. A. Nasseri, B. Van de Wiele, G. Durin, B. Van Waeyenberge, and L. Dupré, J. Phys. D: Appl. Phys. **49**, 465003 (2016).
[17] I. Dzyaloshinskii, Zhur. Eksptl'. i Teoret. Fiz. **33**, (1957).
[18] T. Moriya, Phys. Rev. **120**, 91 (1960).
[19] M. Bode, M. Heide, K. von Bergmann, P. Ferriani, S. Heinze, G. Bihlmayer, A. Kubetzka, O. Pietzsch, S. Blügel, and R. Wiesendanger, Nature **447**, 190 (2007).
[20] E. Y. Vedmedenko, L. Udvardi, P. Weinberger, and R. Wiesendanger, Phys. Rev. B **75**, 104431 (2007).
[21] M. Heide, G. Bihlmayer, and S. Blügel, Phys. Rev. B **78**, 140403 (2008).
[22] S. Rohart and A. Thiaville, Phys. Rev. B **88**, 184422 (2013).
[23] A. Thiaville, S. Rohart, E. Jué, V. Cros, and A. Fert, Europhys. Lett. **100**, 57002 (2012).
[24] E. Martinez, S. Emori, and G. S. D. Beach, Appl. Phys. Lett. **103**, 072406 (2013).
[25] E. Martinez, S. Emori, N. Perez, L. Torres, and G. S. D. Beach, J. Appl. Phys. **115**, 213909 (2014).
[26] L. Berger, Phys. Rev. B **54**, 9353 (1996).
[27] S. Zhang and Z. Li, Phys. Rev. Lett. **93**, 127204 (2004).
[28] T. L. Gilbert, IEEE Trans. Magn. **40**, 3443 (2004).
[29] J. C. Slonczewski, J. Magn. Magn. Mater. **159**, L1 (1996).
[30] M. Tsoi, A. G. M. Jansen, J. Bass, W. C. Chiang, M. Seck, V. Tsoi, and P. Wyder, Phys. Rev. Lett. **80**, 4281 (1998).
[31] E. B. Myers, D. C. Ralph, J. A. Katine, R. N. Louie, and R. A. Buhrman, Science **285**, 867 (1999).
[32] G. Tatara, H. Kohno, and J. Shibata, Physics Reports **468**, 213 (2008).
[33] A. Brataas, A. D. Kent, and H. Ohno, Nature Mater. **11**, 372 (2012).
[34] J. C. Slonczewski, J. Magn. Magn. Mater. **195**, 261 (1999).
[35] G. Tatara and H. Kohno, Phys. Rev. Lett. **92**, 086601 (2004).
[36] A. N. Bogdanov and D. A. Yablonskiĭ, Soviet Physics JETP **68**, (1989).
[37] A. N. Bogdanov and U. K. Rößler, Phys. Rev. Lett. **87**, 037203 (2001).
[38] A. Aharoni, J. Appl. Phys. **83**, 3432 (1998).
[39] A. Vansteenkiste, J. Leliaert, M. Dvornik, M. Helsen, F. Garcia-Sanchez, and B. Van Waeyenberge, AIP Adv. **4**, 107133 (2014).
[40] S. Emori, E. Martinez, K.-J. Lee, H.-W. Lee, U. Bauer, S.-M. Ahn, P. Agrawal, D. C. Bono, and G. S. D. Beach, Phys. Rev. B **90**, 184427 (2014).
[41] O. Boulle, L. D. Buda-Prejbeanu, M. Miron, and G. Gaudin, J. Appl. Phys. **112**, 053901 (2012).
[42] S. Pizzini, J. Vogel, S. Rohart, L. D. Buda-Prejbeanu, E. Jué, O. Boulle, I. M. Miron, C. K. Safeer, S. Auffret, G. Gaudin, and A. Thiaville, Phys. Rev. Lett. **113**, 047203 (2014).

[43] N. L. Schryer and L. R. Walker, J. Appl. Phys. **45**, 5406 (1974).

[44] A. Smith, K. K. Nielsen, D. V. Christensen, C. R. H. Bahl, R. Bjørk, and
J. Hattel, J. Appl. Phys. **107**, 103910 (2010).

[45] D. G. Porter and M. J. Donahue, J. Appl. Phys. **95**, 6729 (2004).

[46] A. A. Thiele, Phys. Rev. Lett. **30**, 230 (1973).

- A Lagrangian–based four collective coordinate DW model is presented.

- Improved semi–analytical approach properly treats the effects of DW asymmetry.

- Semi–analytical approach enables accuracy assessment Lagrangian–based models.

- Semi–analytical approach is used to gain understanding of limitations of models.

- DW asymmetry contributes to discrepancy between models and field–driven simulations.